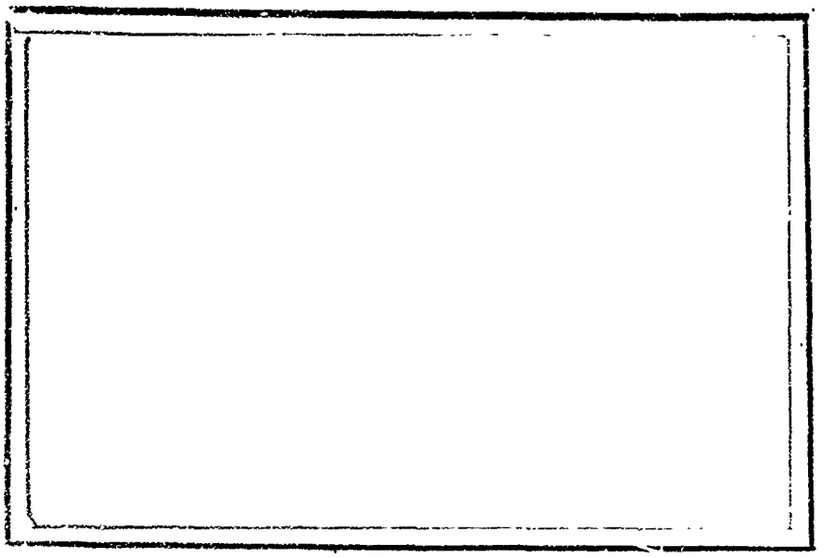

הטכניון – מכון טכנולוגי לישראל
הפקולטה להנדסה אווירונאוטית

TECHNION — ISRAEL INSTITUTE OF TECHNOLOGY
DEPARTMENT OF AERONAUTICAL ENGINEERING
HAIFA, ISRAEL

AF 61(052) – 905
SR – 1
August 1966

SCIENTIFIC REPORT No. 1

GENERAL INSTABILITY OF CYLINDRICAL SHELLS WITH NON-UNIFORM STIFFENERS

Ovadia Harari, Josef Singer and Menahem Baruch

Technion – Israel Institute of Technology
Department of Aeronautical Engineering
Haifa, Israel

TAE REPORT 51

The Research reported in this paper has been sponsored in part by the Air Force Office of Scientific Research OAE under Contract AF 61(052) – 905 through the European Office of Aerospace Research, United States Air Force.

SUMMARY

The present work is a further step towards optimization of stiffened cylindrical shells. Rings and stringers of non-uniform cross-section are analysed as a means of obtaining higher structural efficiencies. For lateral pressure loading, rings with non-uniform height or width are compared. The gain in general instability pressure relative to the uniformly stiffened shell of the same weight amounts to 70 – 80%. For prescribed loading, 10 – 20% weight savings are obtained. For axially compressed cylinders stringers with sinusoidal and linear height variation are studied and compared. Gains in load and weight savings of 30% and 10%, respectively, are obtained, and the sinusoidal variation is found to be superior to the linear variation.

Finally, cylinders under hydrostatic pressure stiffened by a combination of uniform stringers and non-uniform rings are analysed. Different configurations are checked in order to obtain the highest possible efficiencies.

TABLE OF CONTENTS

LIST OF FIGURES

LIST OF SYMBOLS

A_n, B_n, C_n	coefficients of displacement
A_1, A_2	cross-sectional area of stringer and ring
a, b	distances between stiffeners (see Fig. 1)
a_n, b_n	defined by Eqs. (25)
c_{01}, c_{02}	height of the uniform part of stringers and rings respectively (see Fig. 2)
c_1^*, c_2^*	maximum height of the non-uniform part of stiffeners (see Fig. 2)
c_1, c_2	total height of stiffener (see Fig. 1)
$\bar{c}_1$, $\bar{c}_2$	height of the equivalent stiffener
d_2^*	maximum width of the non-uniform part of rings
d_1, d_2	total width of stiffener
$\bar{d}_2$	width of the equivalent ring
D	$\frac{Eh^3}{12(1-\nu^2)}$
D_{0n}, D_{1n}, D_{2n}	defined by Eqs. (25)
E	modulus of elasticity
e_1, e_2	distance between centroid of stiffener cross-section and middle surface of shell
f_1, f_2, f_3	defined by Eqs. (15)

g_1, g_2, g_3	defined by Eqs. (16)
F_A, F_B, F_C G_A, G_B, G_C H_A, H_B, H_C	defined by Eq. (11)
$\bar{G}_B, \bar{G}_C, \bar{H}_B, \bar{H}_C$	defined by Eqs. (D.5)
$\bar{\bar{F}}_A, \bar{\bar{F}}_C, \bar{\bar{H}}_A, \bar{\bar{H}}_C$	defined by Eq. (E.5)
G_B', G_C', H_B', H_C'	defined in Appendix F
$[F_A^*], [F_B^*], [F_C^*]$ $[G_B^*], [G_C^*]$	matrices defined in Appendix C
G	shear modulus
h	thickness of shell
$\bar{h}$	$h\left[1+\frac{c_1 d_1}{hb}+\frac{c_2 d_2}{ha}\right]$
$I_1(n,m), I_2, I_3, I_4$	integrals defined by Eqs. (15)
I_{01}, I_{02}	moment of inertia of stiffener cross-section about the middle surface of the shell
I_{t1}, I_{t2}	torsion constant of stiffener cross-section
k	defined by Eq. (33)
k_1, k_2, k_3, k_4	correcting coefficients
K_1, K_2, K_3	integrals defined by Eq. (D-17)

L	Length of shell between the bulkheads
L_1, L_2, L_3	defined by Eq. (D.13) and Eq. (E.11)
$\bar{L}_1, \bar{L}_2, \bar{L}_3, \bar{L}_4$	defined by Eq. (E.18)
$[M], [\bar{M}], [N]$	matrices defined in Appendix C
$M_x, M_\phi, M_{x\phi}$	moment resultants acting on element
m	integer
$N_x, N_\phi, N_{x\phi}$	membrane force resultants acting on element
$N_{xe}, N_{\phi e}$	error forces defined by Eqs. (20) and (21).
$\bar{N}_x, \bar{N}_\phi$	corrected membrane forces
$N_{x0}, N_{\phi 0}$	prebuckling membrane force resultants
n	number of half longitudinal waves
p	lateral or hydrostatic pressure
P	axial load
$Q(n, m)$	work of the error loads
R	radius of shell
$T(n, m)$	defined by Eqs. (29)
t	number of circumferential waves
u^*, v^*, w^*	displacements (see Fig. 1)
u, v, w	non-dimensional displacements ($=u^*/R$, v^*/R, w^*/R respectively)

x^*, z^*, ϕ	co-ordinates (see Fig. 1)
x, z	non-dimensional co-ordinates
γ	$(1-\nu^2)^{\frac{1}{2}} L^2/Rh$
a, a_1	defined by Eqs. (D,10) or (E.8)
β	$\pi R/L$
γ	variation ratio
$\gamma_{x\phi}$, ϵ_x, ϵ_ϕ	middle surface strains
ζ_1^*, ζ_2^*, η_{01}^*, η_{02}^*, η_{t1}^*, η_{t2}^*	defined in Appendix A
κ_x, κ_ϕ, $\kappa_{x\phi}$	non-dimensional curvature and twist of the middle surface
λ	$= PR/\pi D$
Λ_p	$= pR^3/D$
μ_1^*, μ_2^*, χ_1, χ_2	defined in Appendix A

ν	Poisson's ratio
ψ	defined in Appendix C
∇^4	$(\partial^4/\partial x^4 + 2\partial^6/\partial x^2 \partial \phi^2 + \partial^4/\partial \phi^4)$

SUBSCRIPTS

c.s.	for uniformly stiffened shell
v.s.	for non-uniformly stiffened shell
tr	transition from $n = 1$ buckling shape to $n \neq 1$ buckling shape

Subscripts following a comma indicate differentiation.

1. INTRODUCTION

Experimental and theoretical investigations of uniformly stiffened cylindrical shells with closely spaced heavy stiffeners, [1] to [6], have shown that for axial compression, lateral pressure or torsion, the deflection shape during general instability consists of one half wave in the axial direction. Exceptions to this rule are the cases of ring stiffened shells under axial compression or hydrostatic pressure, in which buckling occurs with many waves, see [1] and [3].

One approach to higher structural efficiencies is to use non-uniform stiffeners, the intensity of which has a maximum at the mid-length of the shell. A similar approach used earlier in optimum design of columns [7] and stiffened plates [8] achieved considerable weight savings by variation of bending stiffness along the length or width of the structure.

In shells, this variation in stiffness can be obtained in two ways: with uniform stiffeners and varying spacing, or with uniform spacing and varying stiffener cross-section. Obviously, a combination of both is also possible. One may note that on account of edge effects both unstiffened and uniformly stiffened cylindrical shells are actually structures of non-uniform stiffness in the axial direction. Non-uniform distribution of stiffener material can compensate for the edge effects and stiffen the shell at the weakest portion. Hence it represents an approach to optimization.

For a cylindrical shell unequal spacing yields "sub-shells" (between rings) of non-uniform buckling strength. The sub-shell next to the bulkheads, where the largest spacing occurs is the most prone to buckling. The increase in general instability will therefore be overshadowed by a decrease in local stability. This argument has to be born in mind all along the analysis since optimization is here mainly concerned with general instability. In contrast to cylindrical shells, conical shells are examples of structures where non-uniform ring spacing is very efficient. In [9] and [10] an optimum weight analysis yielded weight savings of more than 25% for non-uniform ring spacing.

Variation of stiffener cross-section is the alternative method of stiffness variation along the length. In cylindrical shells, such an approach to general instability optimization does not influence the instability of the sub-shells. It is assumed that the influence of stiffener rigidity on local shell instability is small. Since local stiffener instability is rarely a design criterion, the change in stiffener buckling strength is not considered.

The theoretical analysis was performed on st gers and rings of rectangular cross section. The height or width of the stiffeners may be changed along the generator. In some cases a combination of both variations yields the most efficient structure. Some typical variations of stiffeners are shown in Fig. 2. Note that in practical designs only part of the width or height of the stiffeners is varied. Height variation is clearly more effective since the moment of inertia of the stiffener, which determines its main contribution to the stiffness of the shell, varies according to the third power of the height. The maximum permissible height is, however, fixed by practical considerations, such as for example:

1. The thickness of commercially available plates for stiffened cylinders of integral construction.
2. The maximum feasable slenderness ratios.

These constraints are sometimes so severe that the relatively inefficient width-variation is preferable. It may be mentioned that the machining difficulties which arise in the case of height variation do not appear in the case of width variation.

Both types of cross-section variation and different laws for this variation (linear, sinusoidal, see Fig. 2) are considered. The type of stiffeners to be used (rings, stringers or combination of both) depends mainly on the external loading. For lateral pressure and torsion, rings alone are the most efficient, see [1] and [2] while for axial compression a combination of rings and stringers is the best, [10] and [18].

2. THEORETICAL ANALYSIS

2.1. DIFFERENTIAL EQUATIONS AND BOUNDARY CONDITIONS.

The analysis starts with the same main assumptions as [11]. For the sake of clarity they are repeated here.

a) The stiffeners are distributed, or "smeared", over the whole surface of the shell. A more rigorous analysis that takes the discreteness of stiffeners into account is given in [12] and [13]. It is shown there that unless the number of rings is less than 3–4 the difference between the buckling load predicted by "distributed" and "discrete" theories is negligeable.

b) The normal strains ϵ_x and ϵ_ϕ vary linearly in the stiffener as well as in the sheet. The normal strains in the stiffener and in the sheet are equal at their point of contact.

c) The stiffeners do not transmit shear. The shear membrane force $N_{x\phi}$ is carried entirely by the sheet.

d) The torsional rigidity of the stiffener cross-section is added to that of the sheet (the actual increase in torsional rigidity is larger that that assumed).

e) The strain displacement relations are similar to those used by Donnell in [14].

The equations of equilibrium for buckling under axisymmetrical loading are

$$\begin{aligned} &N_{x,x} + N_{x\phi,\phi} = 0 \\ &N_{\phi,\phi} + N_{x\phi,x} = 0 \\ &M_{x,xx} + M_{\phi,\phi} + M_{\phi x,x\phi} - M_{x\phi,x\phi} + RN_{\phi} + RN_{x0}\, w_{,xx} + RN_{\phi 0}\, w_{,\phi\phi} = 0 \end{aligned} \tag{1}$$

where z, x and ϕ are non-dimensional co-ordinates (see Fig. 1).

The stress-strain relations differ for shell and stiffeners and are

$$\left.\begin{aligned} \sigma_x(z) &= [E/(1-\nu^2)][\epsilon_x + \nu\epsilon_\phi - z(\kappa_x + \nu\kappa_\phi)] \\ \sigma_\phi(z) &= [E/(1-\nu^2)][\epsilon_\phi + \nu\epsilon_x - z(\kappa_\phi + \nu\kappa_x)] \end{aligned}\right\} \text{ – in the shell}$$

$$\left.\begin{aligned} \sigma_x(z) &= E(\epsilon_x - z\kappa_x) \\ \sigma_\phi(z) &= E(\epsilon_x - z\kappa_\phi) \end{aligned}\right\} \text{ – in the stiffeners} \tag{2}$$

Note that in Eqs. (2) the middle surface of shell is used as reference line. Hence, the forces and moments acting on an element become

$$\begin{aligned} N_x &= [Eh/(1-\nu^2)]\{\epsilon_x[1 + \mu_1^*(x)] + \nu\epsilon_\phi - \kappa_x\chi_1^*(x)\} \\ N_\phi &= [Eh/(1-\nu^2)]\{\epsilon_\phi[1 + \mu_2^*(x)] + \nu\epsilon_x - \kappa_\phi\chi_2^*(x)\} \\ N_{x\phi} &= [Eh/2(1+\nu)]\,\gamma_{x\phi} \\ M_x &= -(D/R)\{\kappa_x[1 + \eta_{01}^*(x)] + \nu\kappa_\phi - \epsilon_x\zeta_1^*(x)\} \\ M_\phi &= -(D/R)\{\kappa_\phi[1 + \eta_{02}^*(x)] + \nu\kappa_x - \epsilon_\phi\zeta_2^*(x)\} \end{aligned} \tag{3}$$

$$M_{x\phi} = D/R\,[1-\nu+\eta_{t1}^{*}(x)]\,\kappa_{x\phi}$$
$$M_{\phi x} = -(D/R)\,[1-\nu+\eta_{t2}^{*}(x)]\,\kappa_{x\phi} \qquad (3)$$

The curvatures in Eqs. (2) and (3) are non-dimensional, the physical parameters having been divided by R. $\mu_1^{*}(x)$, $\mu_2^{*}(x)$, $\eta_{01}^{*}(x)$, $\eta_{02}^{*}(x)$, $\eta_{t1}^{*}(x)$ and $\eta_{t2}^{*}(x)$ are the changes in stiffness due to non-uniform stringers and rings while $\chi_1^{*}(x)$, $\chi_2^{*}(x)$, $\zeta_1^{*}(x)$ and $\zeta_2^{*}(x)$ represent similar contributions due to the eccentricity of stiffeners (positive for inside stiffeners and negative for outside ones). Their definitions in terms of stiffener geometry for any type of cross-section and for the particular case of rectangular cross-section are given in Appendix A. Note that for constant stiffener cross-section Eqs. (3) degenerate to Eqs. (5) and (6) of [11].

The strains and curvatures are defined, as in [14], by:

$$\begin{aligned}
\epsilon_x &= u_{,x}\\
\epsilon_\phi &= v_{,\phi} - w\\
\gamma_{x\phi} &= u_{,\phi} - v_{,x}\\
\kappa_x &= w_{,xx}\\
\kappa_\phi &= w_{,\phi\phi}\\
\kappa_{x\phi} &= w_{,x\phi}
\end{aligned} \qquad (4)$$

Substitution of Eqs. (3) and (4) into Eqs. (1) yields the equations of equilibrium in terms of displacements

$$u_{,xx} + [(1-\nu)/2]\,u_{,\phi\phi} + [(1+\nu)/2]\,v_{,x\phi} - \nu w_{,x} + [u_{,x}\mu_1^{*}(x)]_{,x} - [w_{,xx}\chi_1(x)]_{,x} = 0$$

$$v_{,\phi\phi} + [(1-\nu)/2]\,v_{,xx} + [(1+\nu)/2]\,u_{,x\phi} - w_{,\phi} + (v_{,\phi\phi} - w_{,\phi})\,\mu_2^{*}(x) - w_{,\phi\phi\phi}\,\chi_2^{*}(x) = 0$$

$$\nabla^4 w + [w_{,xx}\eta_{01}^{*}(x)]_{,xx} - [u_{,x}\zeta_1^{*}(x)]_{,xx} + w_{,\phi\phi\phi\phi}\eta_{02}^{*}(x) + 2\,(w_{,\phi\phi} - v_{,\phi\phi\phi})\,\zeta_2^{*}(x) +$$

$$+ [w_{,x\phi\phi}[\eta_{t1}^{*}(x) + \eta_{t2}^{*}(x)]]_{,x} + 12(R/h)^2[(w-v_{,\phi})[1+\mu_2^{*}(x)] - \nu u_{,x}] + (pR^3/D)w_{,\phi\phi} + (PR/2\pi D)w_{,xx} = 0 \qquad (5)$$

The prebuckling membrane stresses for a combination of axial and lateral loadings are:

$$N_{x0} = -(P/2\pi R)$$
$$N_{\phi 0} = -pR \tag{6}$$

Equations (5) are a set of three linear homogenous partial differential equations with varying coefficients. The usual simply supported boundary conditions are assumed:

$$\left.\begin{aligned} M_x = N_x &= 0 \\ w = v &= 0 \end{aligned}\right\} x = 0 \text{ and } L/R \tag{7}$$

Two methods of solution are proposed. In the first, a straightforward Galerkin procedure is applied to the three equations transforming them into infinite sets of linear algebraic equations. The second employs an approximate procedure which "corrects" the first two stability equations and then solves the third one by a Galerkin procedure. Numerical comparisons between both methods are carried out.

2.2. SOLUTION BY GALERKIN'S METHOD

The variational equivalent of Eqs. (5) is written as

$$\int_0^{L/R}\int_0^{2\pi} \{u_{,xx} + [(1-\nu)/2]\,u_{,\phi\phi} + [(1+\nu)/2]\,v_{,x\phi} - \nu w_{,x} + [u_{,x}\mu_1^*(x)]_{,x} - [w_{,xx}\chi_1^*(x)]_{,x}\}\delta u\, dx\, d\phi = 0$$

$$\int_0^{L/R}\int_0^{2\pi} \{v_{,\phi\phi} + [(1-\nu)/2]\,v_{,xx} + [(1+\nu)/2]\,u_{,x\phi} - w_{,\phi} + (v_{,\phi\phi} - w_{,\phi})\,\mu_2^*(x) - w_{,\phi\phi\phi}\chi_2^*(x)\}\,\delta v\, dx\, d\phi = 0$$

$$\int_0^{L/R}\int_0^{2\pi} \Big\{\nabla^4 w + [w_{,xx}\,\eta_{01}^*(x)]_{,xx} - [u_{,x}\zeta_1^*(x)]_{,xx} + w_{,\phi\phi\phi}\,\eta_{02}^*(x) + 2(w_{,\phi\phi} - v_{,\phi\phi\phi})\,\zeta_2^*(x) +$$
$$+ \{w_{,x\phi\phi}[\eta_{t1}^*(x) + \eta_{t2}^*(x)]\} + 12\,(R/h)^2\{(w - v_{,\phi})[1 + \mu_2^*(x)] - \nu u_{,x}\} + (pR^3/D)\,w_{,\phi\phi} +$$
$$+ (PR/2\pi D)\,w_{,xx}\Big\}\,\delta w\, dx\, d\phi = 0 \tag{8}$$

The displacement components are expanded into Fourier series in the axial direction

$$u = \sin t\phi \sum_{n=1}^{\infty} A_n \cos n\beta x$$

$$v = \cos t\phi \sum_{n=1}^{\infty} B_n \sin n\beta x \qquad (9)$$

$$w = \sin t\phi \sum_{n=1}^{\infty} C_n \sin n\beta x$$

Series (9) fulfil the boundary conditions, Eqs. (7).

A permissible variation of Eqs. (9) is

$$\delta u_m = \sin t\phi \cos m\beta x \, \delta A_m$$

$$\delta v_m = \cos t\phi \sin m\beta x \, \delta B_m \qquad (10)$$

$$\delta w_m = \sin t\phi \sin m\beta x \, \delta C_m$$

Substitution of Eqs. (9) and (10) into Eqs. (8) yields

$$\sum_{n=1}^{\infty} [A_n F_A(n,m) + B_n F_B(n,m) + C_n F_C(n,m)] \delta A_m = 0$$

$$\sum_{n=1}^{\infty} [A_n G_A(n,m) + B_n G_B(n,m) + C_n G_C(n,m)] \delta B_m = 0 \qquad (11)$$

$$\sum_{n=1}^{\infty} [A_n H_A(n,m) + B_n H_B(n,m) + C_n H_C(n,m)] \delta C_m = 0$$

where the F's, G's and H's are defined as

$$F_A(n,m) = [n^2\beta^2 + [(1-\nu)/2] t^2] \delta_{nm} + nm\beta^2 I_1(n,m)$$

$$F_B(n,m) = G_A(n,m) = [(1-\nu)/2] tn\beta \delta_{nm} \qquad (12)$$

$$F_C(n,m) = H_A(m,n) = \nu n\beta \delta_{nm} - n^2 m\beta^3 I_2(n,m)$$

$$G_B(n,m) = [t^2 + [(1-\nu)/2] n^2\beta^2] \delta_{nm} + t^2 K_1(n,m)$$

$$G_C(n,m) = H_B(n,m) = t[\delta_{nm} + K_1(n,m)] - t^3 K_2(n,m) \qquad (13)$$

$$H_C(n,m) = \{1 + [t^2 + n^2\beta^2)^2/12(R/h)^2] - [(\lambda_p t^2 + \lambda n^2\beta^2/2)/12(R/h)^2]\}\,\delta_{nm} - 2t^2 K_2(n,m) +$$

$$+ K_1(n,m) + t^4 K_3(n,m) + \{[n^2 m^2 \beta^4 I_3(n,m) + t^2 n m \beta^2 I_4(n,m)]/12(R/h)^2\} \qquad (14)$$

λ_p and λ are non-dimensional lateral and axial loading parameters respectively. $I_j(n,m)$ and $K_j(n,m)$ are weighted integrals of the functions describing the variation of stiffener cross-section. They are defined by

$$K_j(n,m) = (2\beta/\pi)\int_0^{(\pi/\beta)} f_j(x)\sin n\beta x \sin m\beta x\,dx \qquad j = 1,2,3$$

$$f_1(x) = \mu_2^*(x) \qquad f_2(x) = \chi_2^*(x) \qquad f_3(x) = \eta_{02}^*(x)$$

$$I_1(n,m) = (2/m\pi)\int_0^{(\pi/\beta)} [\mu_1^*(x)\sin n\beta x]_{,x}\cos m\beta x\,dx$$

$$I_2(n,m) = (2/m\pi)\int_0^{(\pi/\beta)} [\chi_1^*(x)\sin n\beta x]_{,x}\cos m\beta x\,dx \qquad (15)$$

$$I_3(n,m) = -(2/m^2\pi\beta)\int_0^{(\pi/\beta)} [\eta_{01}^*(x)\sin n\beta x]_{,xx}\sin m\beta x\,dx$$

$$I_4(n,m) = -(2/m\pi)\int_0^{(\pi/\beta)} [(\eta_{t1}^*(x) + \eta_{t2}^*(x))\cos n\beta x]_{,x}\sin m\beta x\,dx$$

In all derivations it was tacitly assumed that the functional variation of the stiffener cross section is a function of Class 2 (continuous up to derivatives of the second order) otherwise some of the integrals of Eqs. (15) are meaningless. Note that the linear variation (see Fig. 2) exhibits a discontinuity in slope at $x = L/2R$. This case and ones with a similar type of discontinuity, must be handled by a different method. Eqs. (5) which include derivatives of the functional variation, have different meanings when x is on the right or when it is on the left of the discontinuity. A detailed analysis for such cases, that assumes symmetry of stiffener distribution relative to $x = L/2R$, is given in Appendix B.

After repeated integration by parts of Eqs. (15), the final results are

$$\left.\begin{aligned} K_j(n,m) &= (2\beta/\pi)[1 + (-1)^{n+m}]\int_0^{(\pi/2\beta)} f_j(x)\sin n\beta x \sin m\beta x\,dx \\ I_j(n,m) &= (2\beta/\pi)[1 + (-1)^{n+m}]\int_0^{(\pi/2\beta)} g_j(x)\sin n\beta x \sin m\beta x\,dx \end{aligned}\right\} j = 1, 2, 3 \qquad (16)$$

$$I_4(n,m) = (2\beta/\pi)[1+(-1)^{n+m}] \int_0^{(\pi/2\beta)} [\eta_{t1}^*(x) + \eta_{t2}^*(x)] \cos n\beta x \cos m\beta x \, dx$$

$$g_1(x) = \mu_1^*(x) \qquad g_2(x) = \chi_1^*(x) \qquad g_3(x) = \eta_{01}^*(x) \tag{16}$$

Eqs. (16) apply to variation of stiffener cross section with continuous or discontinuous slopes. If one now returns to Eqs. (11) and uses the arbitrariness of the variations δA_m, δB_m, δC_m one obtains three sets of linear algebraic equations which can be written in compact form as

$$\begin{bmatrix} F_A & F_B & F_C \\ G_A & G_B & G_C \\ H_A & H_B & H_C \end{bmatrix} \begin{Bmatrix} A_n \\ B_n \\ C_n \end{Bmatrix} = 0 \tag{17}$$

Consideration of only the first N terms of series (9) yields stability determinants Eqs. (17) of order 3N. Each element of Eq. (17) is an N×N square matrix of which only $[H_C]$ contains the external load along its diagonal. The lowest eigenvalue of Eq. (17) yields the critical load for general instability. The integral value of t (the number of circumferential waves) which minimizes the critical load must be used in computations.

According to Eqs. (12), (13), and (14)

$$[G_A] = [F_B] \qquad [H_B] = [G_C] \qquad [H_A] = [F_C]^T \tag{18}$$

In Eqs. (18), $[\ ]^T$ represents the transpose of the matrix and $[H_B]$ and $[G_C]$ are symmetric.

The stability matrix, Eq. (17), is therefore symmetric as would be expected from Maxwell's reciprocal theorem. This symmetry is of great help during the numerical computations. Integrals $I_j(n,m)$ and $K_j(n,m)$, see Eqs. (16) are identically zero for odd values of the integer $(n+m)$. Under these conditions the stability determinant of Eq. (17) can be resolved into two sub-determinants, one of the even components and one of the odd components of the displacements. The two sub-determinants represent symmetric and antisymmetric buckling modes. The critical load has to be computed for both patterns, and the one yielding the lower load is the one to be considered.

As mentioned earlier, the unknown in Eq. (17) appears only in $[H_C]$. This feature is used to

develop a systematic solution of Eq. (17) whose outline is:

1. Application of Gauss's algorithm to reduce the order of matrix from 3N to N

2. Use of an iterative procedure for calculation of the lowest eigenvalue and eigenvector of the reduced matrix.

Details are given in Appendix C.

2.3. THE METHOD OF "CORRECTING COEFFICIENTS"

For a uniformly stiffened cylindrical shell the differential equations of equilibrium, Eqs. (5), in the presence of the boundary conditions for classical simple supports Eq. (7) have a closed form solution, see [3] or [11]. A non-uniform distribution of stiffeners increases the stiffeness of the middle part of the shell relative to that at the edges. During buckling, the deflection curve, which in the case of constant stiffeners is a half sine wave in the axial direction, will be of similar shape with a pronounced flatness at the middle of the shell. If one considers the expressions of displacements, Eqs. (9), this means that the first term of the series is dominant, and the additional terms correct the basic mode only slightly without altering its general features. This is the main assumption of the method of "correcting coefficients" used earlier [15] in connection with general instability of stiffened conical shells. In the application of the method, the varying coefficients of the first two differential equations, Eqs. (5), are changed to constant ones. Substitution of series (9) into the resulting two "corrected" equations generates an infinite set of uncoupled linear algebraic equations. Hence only the general harmonic, n, has to be considered. The third stability equation with increments from the first and the second is solved by a Galerkin procedure.

The variational equivalent of differential equations (I) is

$$\delta v = \int_0^{2\pi}\int_0^{(L/R)} \{[N_{x,x} + N_{x\phi,\phi}]\,\delta u + [N_{\phi,\phi} + N_{x\phi,x}]\,\delta v + [M_{x,xx} + M_{\phi,\phi\phi} - M_{x\phi,x\phi} +$$

$$+ M_{\phi x,x\phi} + RN_{\phi} + RN_{x0}\,w_{,xx} + RN_{\phi 0}\,w_{,\phi\phi}] (\delta w/R)\} R^2\,dx d\phi - \oint_0^{2\pi} \{N_x\,\delta u + N_{x\phi}\,\delta v -$$

$$- (M_x/R)(\delta w)_{,x} + [(M_{x,x}/R) - (M_{x\phi,\phi}/R) + (M_{\phi x,\phi}/R) + N_{x0}\,w_{,x}]\delta w\} R^2\,d\phi \Big|_{x=0}^{x=(L/R)} = 0 \qquad (19)$$

This equivelent is the variation of the generalised potential after two integrations by parts. Since the variations are arbitrary, the differential equations (1) and boundary conditions (7) can readily be obtained from Eqs. (19).

To the membrane forces, defined by Eqs. (3), a set of terms, whose sum is zero is added. Then

$$N_x = [Eh/(1-\nu^2)]\{u_{,x}(1+k_1) + \nu(v_{,\phi} - w) - w_{,xx}k_2\} + [Eh/(1-\nu^2)]\{u_{,x}[\mu_1^* - k_1] -$$

$$- w_{,xx}[\chi_1^*(x) - k_2]\} = \bar{N}_x + N_{xo} \tag{20}$$

where k_1 and k_2 are constants. The second term of the last expression in Eq. (20), N_{xo}, is called "Error Load". Similarly the membrane force N_ϕ is transformed to

$$N_\phi = \bar{N}_\phi + N_{\phi o} = [Eh/(1-\nu^2)]\{(v_{,\phi} - w)(1+k_5) + \nu u_{,x} - k_4 w_{,\phi\phi}\} +$$

$$+ [Eh/(1-\nu^2)]\{(v_{,\phi} - w)[\mu_2^*(x) - k_3] - w_{,\phi\phi}[\chi_2^*(x) - k_4]\} \tag{21}$$

Substitution of Eqs. (20) and (21) into Eq. (19) yields

$$\int_0^{2\pi}\int_0^{(L/R)} \Big\{[\bar{N}_{x,x} + N_{x\phi,\phi}]\,\delta u + [\bar{N}_{\phi,\phi} + N_{x\phi,x}]\,\delta v + [N_{xo,x}\,\delta u + N_{\phi o,\phi}\,\delta v +$$

$$+ [M_{x,xx} + M_{\phi,\phi\phi} + M_{\phi x,x\phi} - M_{x\phi,x\phi} + RN_\phi + RN_{\phi 0}\,w_{,\phi\phi} + RN_{x0}\,w_{,xx}]$$

$$(\delta w/R)\}\Big]\,dx\,d\phi = 0 \tag{22}$$

since the line integral vanishes on account of boundary conditions, Eqs. (7), which are satisfied by the assumed displacement series.

The corrected first two stability equations are then

$$\begin{aligned} \bar{N}_{x,x} + N_{x\phi,\phi} &= 0 \\ \bar{N}_{\phi,\phi} + N_{x\phi,x} &= 0 \end{aligned} \tag{23}$$

Assumption of a solution of the type

$$u = A_n \sin t\phi \cos n\beta x$$

$$v = B_n \cos t\phi \sin n\beta x \tag{24}$$

$$w = C_n \sin t\phi \sin n\beta x$$

and use of Eqs. (20) and (21) yields two homogenous algebraic equations with three unknowns A_n, B_n and C_n, which are related to each other through

$$A_n = a_n c_n \qquad a_n = (D_{1n}/D_{0n})$$

$$E_n = b_n c_n \qquad b_n = (D_{2n}/D_{0n}) \tag{25}$$

where

$$D_{0n} = [(1-\nu)/2](1+k_{\cdot} \qquad (1+k_1)(1+k_3) - \nu]n^2\beta^2 t^2 + [(1-\nu)/2](1+k_1)n^4\beta^4$$

$$D_{1n} = [-(1+\nu)/2]n\beta t^4 k_4 + (1+k_3)[k_2 n^3\beta^3 + [(1-\nu)/2]n\beta]t^2 + [(1-\nu)/2]n^3\beta^3[k_2 n^2\beta^2 - \nu]$$

$$D_{2n} = [(1-\nu)/2]k_4 t^5 + [(1+k_1)n^2\beta^2 k_4 - [(1-\nu)/2](1+k_3)]t^3 + \{[[\nu(1+\nu)/2] -$$

$$(1+k_1)(1+k_3)]n^2\beta^2 - [(1+\nu)/2]k_2 n^4\beta^4\}t \tag{25a}$$

The third equation, with the "Error Loads",

$$0 = \int_0^{2\pi} \int_0^{L/R} \{N_{x\phi,x}\,\delta u + N_{\phi\phi,\phi}\,\delta v + [M_{x,xx} + M_{\phi,\phi\phi} + M_{\phi x,x\phi} - M_{x\phi,x\phi} + RN_\phi +$$

$$+ RN_{\phi 0}\,w_{,\phi\phi} + RN_{x0}\,w_{,xx}](\delta w/R)\}\,dx\,d\phi \tag{26}$$

is solved by a Galerkin procedure. Substitution of Eqs. (25) into the expressions of the displacements, Eqs. (9), and their variations, Eqs. (10), yields

$$u = \sin t\phi \sum_{n=1}^{\infty} a_n C_n \cos n\beta x \qquad \delta u_m = a_m \sin t\phi \cos m\beta x\,\delta C_m$$

$$v = \cos t\phi \sum_{n=1}^{\infty} b_n C_n \sin n\beta x \qquad \delta v_m = b_m \cos t\phi \sin m\beta x\,\delta C_m \tag{27}$$

$$w = \sin t\phi \sum_{n=1}^{\infty} C_n \sin n\beta x \qquad \delta w_m = \sin t\phi \sin m\beta x\, \delta C_m \tag{27}$$

Substitution of Eqs. (20), (21) and (3) in Eq. (26) yields

$$\begin{aligned} 0 = \int_0^{2\pi(L/R)} \int_0^{} \Big\{ & [Eh/(1-\nu^2)] \{ [u_{,x}(\mu_1^*(x) - k_1)]_{,x} - [w_{,xx}(\chi_1^*(x) - k_2)]_{,x} \} \delta u + [Eh/(1-\nu^2)] \\ & \{ (v_{,\phi\phi} - w_{,\phi})[\mu_2^*(x) - k_3] - w_{,\phi\phi\phi}[\chi_2^*(x) - k_4] \} \delta v - (D/R^2) \{ \nabla^4 w + [w_{,xx}\eta_{01}^*(x)]_{,xx} \\ & - [u_{,x}\zeta_1^*(x)]_{,xx} + w_{,\phi\phi\phi\phi}\eta_{02}^*(x) + (2w_{,\phi\phi} - v_{,\phi\phi\phi})\zeta_2^*(x) + [w_{,x\phi\phi}(\eta_{t1}^*(x) + \\ & + \eta_{t2}^*(x)]_{,x} + 12(R/h)^2 [(v_{,\phi} - w)(1 + \mu_2^*(x)) - \nu u_{,x}] + \lambda_p w_{,\phi\phi} + \lambda(w_{,xx}/2) \} \delta w \Big\} dx\, d\phi \end{aligned} \tag{28}$$

Use of Eqs. (27) and the definitions of the weighted integrals, Eqs. (16), yields

$$\sum_{n=1}^{\infty} T(n,m)\, C_n = 0 \qquad m = 1, 2 \ldots\ldots \infty$$

where

$$\begin{aligned} T(n,m) = \Big\{ & Q(n,m) + \{ [(n^2\beta^2 + t^2)/12(R/h)^2] + 1 + b_n t + \nu n\beta a_n - [(\lambda n^2\beta^2/2) + \\ & + \lambda_p t^2]/12(R/h)^2 \} \delta_{nm} + \{ [n^2 m^2 \beta^4 I_3(n,m) + n m \beta^2 t^2 I_4(n,m) + t^4 K_3(n,m)]/12(R/h)^2 \} - \\ & - n m^2 \beta^3 a_n I_2(n,m) - t^2(2 + b_n t) K_2(n,m) + (1 + b_n t) K_1(n,m) \Big\} \end{aligned} \tag{29}$$

$Q(n,m)$ the work done by the error loads, is defined by

$$\begin{aligned} Q(n,m) = & \{ a_n [I_1(n,m) - k_1 \delta_{nm}] - n\beta [I_2(n,m) - k_2 \delta_{nm}] \} n\beta\, m\beta\, a_m + \\ & + \{ (1 + b_n t)[K_1(n,m) - k_3 \delta_{nm}] - t^2 [K_2(n,m) - k_4 \delta_{nm}] \} t b_m \end{aligned} \tag{30}$$

A finite number of terms, N, in Eq. (29) yields a set of N linear homogenous equations. For reasons similar to those presented in the previous section, the determinant can be resolved into sub-determinants of the even and odd components respectively. Again the value of t that minimizes the critical load has to be used.

2.4. EVALUATION OF THE CORRECTING COEFFICIENTS

The accuracy of the method in predicting general instability largely depends on the manner in which the correcting coefficients are computed. In the present solution they are evaluated by equating to zero the work of the error loads, N_{x_0} and N_{ϕ_0}, of the first two stability equations. This work is computed for different permissible displacements in the same modus operandi applied in Galerkin's method. It should be mentioned however that due to the limited number of unknowns (k_1, k_2, k_3 and k_4) the virtual work can be made to vanish for a maximum of four different displacements.

As a first approximation the first terms, $n=1$, of series (27) are used as permissible displacements. Bearing in mind the discussion at the beginning of section 2.3, this choice is very promising, since $n=1$ is the basis mode of the deflection shape during general instability.

The error work expression, Eq. (30), then yields

$$\begin{aligned} k_1 &= I_1(1,1) & k_3 &= K_4(1,1) \\ k_2 &= I_2(1,1) & k_4 &= K_2(1,1) \end{aligned} \tag{31}$$

There are cases, however, where the first term of series (27) is not dominant, e.g. the case of a long stiffened shell under axial compression, then Eqs. (31) will yield very unconservative buckling loads.

A more systematic, though less simple way of computing the correcting coefficients is to use the actual displacements at buckling in the computation of the virtual work. In other words, not the first terms of Eqs. (27) but the whole series are used as permissible displacements.

Then

$$\begin{aligned} k_1 &= \frac{\sum_{n,m=1}^{N} n\, m\, a_n\, a_m\, C_n\, C_m\, I_1(n,m)}{\sum_{n=1}^{N} n^2\, a_n^2\, C_n^2} = \frac{\{n\, a_n\, C_n\}\,[I_1]\,\{n\, a_n\, C_n\}}{\{n\, a_n\, C_n\}\,\{n\, a_n\, C_n\}} \\ k_2 &= \frac{\sum_{n,m=1}^{N} n^2\, m\, C_n\, C_m\, I_2(n,m)\, a_m}{\sum_{n=1}^{N} n^3\, C_n^2\, a_n} = \frac{\{n^2\, C_n\}\,[I_2]\,\{n\, a_n\, C_n\}}{\{n^2\, C_n\}\,\{n\, a_n\, C_n\}} \end{aligned} \tag{32}$$

$$k_3 = \frac{\sum_{n,m=1}^{N} (1 + b_n t)\, C_n\, K_1(n,m)\, b_m\, C_m}{\sum_{n=1}^{N} (1 + b_n t)\, C_n^2\, b_n} = \frac{\{(1 + b_n t)\, C_n\}\, [K_1]\, \{b_n\, C_n\}}{\{(1 + b_n t)\, C_n\}\, \{b_n\, C_n\}}$$

$$k_4 = \frac{\sum_{n,m=1}^{N} C_n\, K_2(n,m)\, b_m\, C_m}{\sum_{n=1}^{N} C_n^2\, b_n} = \frac{\{C_n\}\, [K_2]\, \{b_n\, C_n\}}{\{C_n\}\, \{b_n\, C_n\}} \qquad (32)$$

where $\{\ \}$, $\{\ \}$ are shorthand notation for row and column matrices.

It should be pointed out, however, that preliminary knowledge of the eigenvector is needed in Eqs. (32). Hence an iteration procedure is required. As a first approximation one uses Eqs. (31). The computed eigen-vector is then used in Eqs. (32). The process is repeated until reasonable convergence of the solution is achieved.

The purpose of the method of correcting coefficients was to provide an easier, though less accurate, method for solving the stability equations (5). It lead to an iterative process. In comparing computations for both methods it is obvious that, in the present case, the loss in accuracy in the second method outweighs the numerical difficulties of the first. However, this is not always so, since for other types of shells (conical) or loads (torsion) a straightforward Galerkin or Rayleigh-Ritz procedure might be very cumbersome.

In the present work both methods were used for solving a typical problem. Comparison of the results yielded important information as to the accuracy of the approximate method of "correcting coefficients" and its computional time saving.

3. NUMERICAL RESULTS AND DISCUSSION

3.1. INTRODUCTION

The theoretical analysis considered a general non-uniform distribution of stiffeners, symmetrical with respect to the mid-length of the shell. In order to obtain an estimate of the possible gains in load for a constant structure weight or of the weight saving for a constant load, one must now solve the problem numerically for typical laws of stiffness variation. The cases considered here are:

1) Cylindrical shells subjected to lateral pressure and stiffened by rings of non-uniform width or height.

2) Axially compressed cylindrical shells stiffened by stringers with sinusoidal or linear height variation.

3) Cylindrical shells subjected to hydrostatic pressure and stiffened by a combination of uniform stringers and rings of non-uniform height.

All cases were solved by the more rigorous Galerkin procedure. Case 2 was also solved by the approximate method of "correcting coefficients". The shape of the cross section was assumed rectangular for all stiffeners.

3.2. LATERALLY LOADED CYLINDRICAL SHELL STIFFENED WITH NON-UNIFORM RINGS

3.2.1. APPROXIMATE ANALYSIS

Lateral pressure loading is of less practical importance than hydrostatic pressure but is easier to handle analyticly. Hence it is considered first. Now general instability under lateral pressure occurs, for unstiffened cylindrical shells as well as stiffened ones, with one wave in the axial direction, see [1] and [16]. Hydrostatic pressure is a case of combined loading (axial and lateral pressures) and yields buckling shapes that are combinations of the modes occuring under the axial and lateral components. This interaction was analysed for stiffened shells in [1] for a large range of shell and ring geometries. It was found there that for short and thick shells (small Z) general instability occured with many waves in the axial direction. From these arguments one can qualitatively conclude that, while for lateral pressure rings of non-uniform cross section varying linearly or according to half a sine wave, see Fig. 2, might be very promising, for hydrostatic pressure the same distribution of rings will inevitably lead to large losses of efficiency. This point is later discussed in detail. For cylinders stiffened with rings only, the first set of N algebraic equations in Eqs. (11) uncouple, and hence the order of the stability determinant, Eq. (17), is reduced. For more details, as well as explicit expressions of integrals (16), see Appendix D.

To get an idea of the structural efficiency of non-uniform stiffeners, the case of rings with non-uniform width is first analysed. A closed form solution is possible if one uses the first terms of Eqs. (9)

as a rough approximation to the buckling shape for general instability.

For a width of ring varying according to $f(x)$ along the generator, the weight saving, relative to a uniformly stiffened shell buckling at the same load, is given by

$$\bar{h}_{v.s}/\bar{h}_{c.s} = [1 + (A_2/ah)]/[1 + (kA_2/ah)]$$

where

$$k = (2\int_0^{(\pi/\beta)} f(x)\sin^2\beta x dx)/(\int_0^{(\pi/\beta)} f(x)\,dx) \tag{33}$$

and A_2 is the area of rings for the uniformly stiffened cylinder.

The function $f(x)$ which minimizes the ratio (largest weight saving) was found to be Dirac's delta function.

$$f(x) = \delta[(\pi/2\beta) - x] \tag{34}$$

for which the value of the ratio is

$$\bar{h}_{v.s}/\bar{h}_{c.s} = [1 + (A_2/ah)]/[1 + 2(A_2/ah)] \tag{35}$$

With $A_2/ah = 1$, which represents a typical geometry in aerospace vehicles, a maximum weight savings of 33.3% is then obtained.

Variation of ring width according to Eq. (34) means concentration of the whole stiffener area in one bulkhead at the mid-length of the shell, see Fig. 3. This is the direct result of the approximation assumed at the beginning of this section. The deflecting shape for general instability was assumed a half sine wave ($n = 1$), hence the rings tend to concentrate in the weakest part of the shell – in the middle. The $n = 2$ buckling mode, however, was not taken in account, though in the case presented in Fig. 3 it is the one most prone to occur. The shell will, therefore, buckle locally at a pressure much below that causing general instability of the uniformly stiffened cylinder. The efficiency of non-uniform stiffeners is therefore made up of two opposing contributions. A primary positive contribution resulting from the strengthening of the weak mid-length of the shell, and a secondary negative contribution due to the weakening of the shell close to the edges that may then buckle prematurely. This premature buckling mode will henceforth be called a "many wave" deflection shape in the axial direction.

3.2.2. RINGS OF NON-UNIFORM HEIGHT

In order to obtain a better feeling for the influence of the opposing contributions on structural efficiency, different types of height variation were analysed. In Fig. 4 the non-dimensional ratio $c_2/\bar{c}_2$ that describes the variation of the height of the rings along a generator, is drawn versus x for different values of the parameter γ. γ the "variation ratio" is the ratio between the weight of the uniform part of the ring to their total weight and its values are restricted by the inequality

$$0 < \gamma < 1 \tag{36}$$

$\gamma = 1$ represents the case of uniform stiffeners, while $\gamma = 0$ the one where the entire height of the ring varies ~~accidently~~ with x. The smaller γ the more of the stiffeners weight (which is kept constant for all the values of γ) is near the mid-length of the shell.

In Fig. 5 the radial displacement at buckling is given for a short shell and different values of γ. The parameters e_2/h and A_2/ah are those of the equivalent uniform rings (weight equivalence). This equivalency will be used later on for computing the efficiency of non-uniform stiffeners. For $\gamma = 1$ the deflection is a half sine wave; a decrease in γ distorts the buckling shape so as to flatten its extremum at $x = (L/2R)$. It is worth mentioning that, except slight corrections in shape, the curve still resembles the basic half sine wave in the axial direction. This supports the intuitive argument given in Section 2.3. As γ is further decreased, however, a change in behaviour is observed. For $\gamma = 0.25$ two completely different deflection curves are drawn. One represents the normal shape with one buckle along the generator, whereas the other represents a "multi-wave" behavior with relatively small displacements at the middle of the shell. During the process of minimization of the lowest eigenvalue of (17) relative to t, a double minimum curve is found (see for example Fig. 9). Each of the extremus represents a different buckling mode, and the one yielding the lowest buckling pressure is physically significant. In Fig. 5 both deflection curves were drawn for $\gamma = 0.25$ because they both occured at almost the same value of the external pressure. (The difference in λ_p was of the order of 0.9%). For $\gamma = 0$ the $n \neq 1$ buckling mode is dominant.

In Figs. 6 and 7 the radial displacements are given for two other shells of different geometry. The longer the shell the more pronounced is the mode change. The term "edge buckling" can be ap-

plied to the "multi-wave" buckling pattern in the sense that very rapid changes in the displacements take place in the neighbourhood of the edges. The magnitude of the displacements is zero for more than 70% of the length of the shell. In Fig. 7 two curves are again drawn for $\gamma = 0.25$ for the same reason as before in Fig. 5.

In Table 1 the computed eigen-vectors are given for the deflection shapes of Fig. 7. For $\gamma = 0$ and 0.25 the two columns, represent two possible buckling shapes. The first is the so-called "n = 1" mode of instability. This name is fully justified since C_1 is much larger than the other coefficients. The second column represents the $n \neq 1$ buckling shape. It is characterised by:

a. poor convergence of the stability determinant, Eq. (17);

b. a large number of circumferential waves (see table 1);

c. none of the terms of the displacement series, Eqs. 9, dominates.

For the particular case $\gamma = 0$ the terms C_9, C_{11} and C_{13} are of similar magnitude.

In Fig. 8 the deflection curves for the same geometries of shell and rings as in Fig. 6 are given for outside rings ($e_2/h < 0$). There is a noticeable influence of the eccentricity on the efficiency of the non-uniform variation of stiffeners. A comparison of Figs. 6 and 8 shows that for outside rings the "multi-wave" buckling shape is postponed to lower values of γ. As will be seen later, this increases the gain in load.

Figs. 5 to 8 clearly show that from a certain value of γ (the actual value depends on the shell geometry) down, an "edge buckling" pattern dominates, leaving the middle part of the shell relatively underformed. Numerical results for this "edge buckling" mode show large losses in efficiency. The buckling load amounts to less than 50% of that obtained with uniform stiffeners. The physical argumeats behind those losses are similar in nature to those presented in the analysis of Eq. (34). In other words, the overstiffening of the middle part of the shell leaves the neighbourhood of the edges relatively weak and therefore very prone to buckling.

In Fig. 10 the gain in load $p_{v,s}/p_{c,s}$ is drawn versus γ for different shell geometries. Most of the curves have a discontinuity in slope at certain values of γ that may be denoted γ_k. For $\gamma > \gamma_k$ the deflections during buckling have one basic wave along the generator. Decrease in γ from $\gamma = 1$ to γ_k results in a monotonous increase of the gain in load. To the left of the discontinuity the "edge buckling" pattern dominates, leading to losses in efficiency.

For $\gamma = \gamma_{cr.}$ one obtains the highest gains in load for a certain shell geometry. Its value varies with Z. For very short shells, for example, no "multi-wave" pattern takes place and therefore, $\gamma_{cr.} = 0$ is the optimum variation ratio.

In Fig. 11 the optimum gain in load, obtained at $\gamma = \gamma_{cr.}$ (see Fig. 10), is plotted versus the shell geometry parameter Z. For very low values of Z, $Z < 30$. $\gamma_{cr.}$ is zero. In the intermediate range $30 < Z < 100$ very rapid changes occur in the value of $\gamma_{cr.}$ causing the changes in curvature that appear in Fig. 11. Further away from the perturbed region the rise of the curve is monotonous. It should be noted that for long shells, the mode transition is very sharp, see Fig. 10, and causes very large losses in efficiency. A small margin of safety is, therefore, advisable and variation ratios slightly larger than $\gamma_{cr.}$ should be employed. The larger gains in load obtained with outside rings are somewhat overshadowed by the superiority of uniform inside rings over outside ones, see [1].

In most problems of practical interest the geometry of the shell as well as the applied loads are given. The designers' job is to find the configuration of stiffeners yielding minimum weight. Care should be taken about physical and practical constraints such as yielding of material, maximum permissible ring or stringer height, etc.

The procedures described in Chapter 2 for solving differential equations (5) are often known as the "direct" problem: Computation of the load causing general instability for given stiffener and shell geometry. The "indirect" problem of finding the ring geometry for a given load is in general more difficult. One assumes different values for the ring geometry and computes the corresponding values of the buckling load with one of the methods of Chapter 2. When these values are close enough to the load given in the data, a regular-falsi method is used to increase the convergence of solution.

In Fig. 11 the weight saving equivalent of the gain load, given by the full curves, is plotted versus Z. Its magnitude is never larger than 10–15%. It should be carefully noted that the present analysis is not an optimization procedure in the sense of [17] and [18] because:

a. only general instability of the composite structure is analysed,

b. the weight minimization is on stiffener configuration only, whereas the thickness of shell is kept constant

In Fig. 11 the weight of the rings is only 1/3 of the total weight ($A_2/a = h/2$). Therefore, saving

15% in the total weight of the shell, by using non-uniform stiffeners, is equivalent to a 40% saving in the weight of the rings.

The structural efficiency depends to a large extent on the area ratio of the rings (A_2/ah), and the larger the area ratio the larger are the weight savings. Typical computations have shown that for $(A_2/ah) = 1$ they amount to 20–25% of the original weight of the uniformly stiffened shell.

In Fig. 12 and Table 2 the gain in load is plotted versus Z for different values of γ. The first two curves for $\gamma = 0.75$ and 9.5 show a continuous, monotonous rise of efficiency with Z. The radial displacements at buckling have one lobe in the axial direction. For $\gamma = 0.25$ the curve for inside rings has two discontinuities in slope. In the intermediate range of Z, the "edge buckling" pattern dominates and causes losses in efficiency. It should be mentioned that the curve for outside rings and the same value of γ is continuous. The curves for $\gamma = 0$ are mainly of academic interest, since they emphasize the consequences of understiffened edges on general instability.

In Fig. 13 and 14 the influence of ring cross-sectional area A_2 and magnitude of eccentricity (e_2/h) on the gain in load is investigated. Comparing respective curves in Fig. 12 and 13 shows small differences in gain. On the other hand, the curves in Fig. 14 are of somewhat different nature. The "edge buckling" pattern appears already for $\gamma = 0.5$, while for $\gamma = 0.25$ its zone of influence extends to a larger range of Z. This is not surprising since increasing the equivalent height of rings from $(e_2/h) = 5$ to $(e_2/h) = 10$ results in overstiffening the middle part of the shell. A clearer picture is obtained in Fig. 15 where the gain is plotted for different values of (e_2/h) and a constant γ. For $(e_2/h) = 3$ the curve is continuous with relatively high gains for all the spectrum of Z. For the other values of (e_2/h) the efficiency gradually decreases and may even change its sign. While Fig. 15 analyses the influence of (e_2/h) on the "edge buckling" pattern, Fig. 16 does the same for a pattern with one buckle along the x axis. For long shells (large Z) Fig. 16 shows larger gains in load the larger the eccentricity. In the left part of the figure (small Z) the behavior of the curves is similar that in Fig. 15.

3.2.3. RINGS OF NON-UNIFORM WIDTH

When comparing a height and width variation of rings, the superiority of the first is almost

obvious, since the stiffening material is then used in a more efficient way. In many cases, however, practical constraints rule out the use of height variation, leaving only width variation as a possible method of optimization. The explicit formulation of integrals (16) for a sinusoidal width variation is given in the third section of Appendix D. The absence of stringers simplifies Eqs. (12) yielding $2N \times 2N$ stability determinant. The algebraic details are similar to those given for height variation (see Appendix C).

Numerical results show that in the present case a variation ratio $\gamma = 0$ yields, at buckling, a deflection shape with one lobe in the axial direction. Computations were carried out for a large spectrum of shell and ring geometries.

For larger values of γ the same mode persists leading to a gradual decrease in efficiency. Hence only the optimum γ is used in the computations. It may be recalled that in the case of height variation of rings, $\gamma = 0$ yielded very low efficiencies. If one aims at a physical explanation of the difference between both variations, one finds that a non-uniform width understiffens the edges in a milder way postponing the appearance of the "edge buckling" pattern. In the mathematical formulation, the difference between width or height variation according to $\sin \beta x$ lies in the fact that the bending stiffness of the ring changes according to $\sin \beta x$ and $\sin^3 \beta x$ respectively. The intensity of the non-uniform distribution at the edge of the shell, given by the slope of the $\sin \beta x$ and $\sin^3 \beta x$ curves is, therefore, finite for width variation and zero for height variation. Since this slope is of critical importance for the "edge buckling" pattern, the difference in behavior is apparent. In Fig. 17 and Table 2 the gain in load and weight saving are plotted versus Z for inside and outside rings. Comparison of the results with the optimum gains obtained for height variation, see Fig. 11, confirms the intuitive conclusions reached at the beginning of the section. In Fig. 17 the maximum gains in load are of the order of $15-20\%$, much lower than those for the height variation. The weight savings on the other hand are of the same order of magnitude. This is not surprising since the weight optimization was performed in each case with different constraints. For rings of non-uniform width, the efficiency of stiffeners was compared with that of uniform rings of the same height and equivalent width. For height variation the equivalency was related to the height, while the width was kept constant.

3.3. AXIALLY LOADED CYLINDRICAL SHELL STIFFENED BY NON-UNIFORM STRINGERS

Recent optimization studies on axially loaded cylindrical shells [10] and [18] have shown that a combination of rings and stringers yield the highest structural efficiency. In the present analysis only the influence of non-uniform stringers is studied in detail. That of rings alone, is of no interest, since alone they are very inefficient for this type of loading. An optimization with both non-uniform stringers and rings could yield further gains, but is not considered in this report. Sinusoidal and linear height variations (see Fig. 2) were analysed in order to study the influence of the functional variation on structural efficiency. A width variation of stringers is of little interest since it yields gains in load of only few percents. In the case of stringer-stiffened shells every term of the displacement series, Eqs. 9, is a possible solution of the second stability equation, Eqs. (5). By relatively simple manipulations, the order of the matrix, Eq. (17), can be reduced to 2N. Further details, as well as the explicit expressions of integrals (16) for the two types of variation, are given in Appendix E.

In Fig. 18 and Table 3 the influence of shell geometry on the structural efficiency of non-uniform stringers is studied for different values of γ. For $\gamma = 0.75$ and 0.5 the curves drop monotonously to asymptotic value $p_{v,s}/p_{c,s} = 1$. For long shells ($Z > 5000$) stiffened by inside stringers, the gains in load do not justify the increase in the cost of production due to non-uniform stringers. It should be mentioned, that in the same range of Z, even uniform stiffeners are less efficient than equivalent thickening of shell, see [3]. Comparing the gains in load for ring-stiffened shells, Fig. 12, and stringer-stiffened ones, Fig. 18, one observes, in addition to the difference in magnitude, that the behavior with increase in Z is reversed.

For $\gamma = 0.25$, and even more so for $\gamma = 0$ (see Table 2), an "edge buckling" pattern, similar to the one occuring in ring stiffened shells, dominates, causing a very rapid decrease in structural efficiency. The reduction is even more pronounced than that occuring in Fig. 12, because of the different buckling behaviors of isotropic shells under lateral and axial loadings. For large values of Z (long shells), the single "half wave" buckling pattern is once again dominant (even for $\gamma=0$), yielding higher gains for lower values of γ.

For small values of Z ($Z < 100$), cylindrical shells stiffened with outside stringers buckle in an axisymmetric mode, see also [3], causing a large scatter of the computed points. The curves in Fig.

18 smooth out the effect of this scatter. In Fig. 18 the influence of eccentricity on structural efficiency is also investigated. For values of Z smaller than 1000, the gains in load are higher for inside stringers. An inversion occurs at larger Z values, yielding noticeable differences between the efficiency of both configurations. For a typically long shell, (L/R) = 2, (R/h) = 1000, the gain in load is increased from 2% to 15% by changing the position of the stiffeners. It should also be mentioned that recent experimental and theoretical investigations, [3] to [6], emphasize the superiority of uniform outside stringers over inside ones. In Fig. 19 the influence of the magnitude of eccentricity on the gain in load is investigated. Since a variation ratio $\gamma = 0.5$ is used, "edge buckling" is eliminated as a possible mode of instability. Increase in the magnitude of eccentricity for a constant stringer area, yields more slender stiffeners, whose height increases in inverse proportion to the decrease of the width. As a result, the moment of inertia of stiffener cross section varies according to:

$$(I_{11}/bh^3) \propto (e_1/h)^2$$

The gains in load, which are in direct proportion to the bending stiffeness of the stringers, grow larger, the larger the eccentricity. However, practical considerations prescribe upper limits to the magnitude of e_1/h. Some of them are:

a) local buckling of stiffener as a simply supported – free plate,

b) the thickness of commercially available sheets,

c) reduction of the width of the stringer d_1 (see Fig. 1) beyond a certain limit, reduces the "effective width" of the sheet between the stiffeners. The present analysis does not account for the resulting decrease in the total stiffeness of the shell.

In Fig. 20 the influence of γ on the gain in load is investigated for two types of non-uniform height variation. In the neighbourhood of $\gamma = 1$, the two variations yield similar results. With decrease in γ the gain in load increases and goes through a maximum, which represents a general characteristic behavior of non-uniform stiffeners. In the case of rings, this maximum appeared as a discontinuity in slope, see Fig. 10. This discontinuity is caused by transition from an "edge buckling" pattern to a single half wave pattern in the axial direction. In the present case of stringers, however, the transition is continuous. For sinusoidal height variation the optimum value of γ is lower than for the linear one, yielding therefore higher gains in load. Physically, this means that the linear variation is more prone

to "edge buckling" and "needs" larger parts of the stringer to be uniform along the shell. The optimum γ at which the maximum gains are obtained varies with the shell geometry. For long shells (large Z) it has a tendency to move to the left of Fig. 20 until a value of Z is reached ($Z \approx 10^4$) for which $\gamma = 0$ is the best configuration. In the "short shell" range $Z < 10^3$ higher values of γ are needed to increase the stiffness in the axial direction.

In Fig. 21 the two types of stiffener variation are compared for different shell geometries. While for $\gamma = 0.75$ the linear variation is superior, the opposite holds for $\gamma = 0.5$ and 0.25.

For axially compressed isotropic thin cylindrical shells the experimental buckling stresses are much below those computed by small deflection theory. Recent experimental results [4] [6] and [19] have, however, shown that heavily stiffened shells can be adequately analysed by linear theory. With closely spaced and relatively large stiffeners, experimental results fall within a few percent of the theoretically computed loads. For small values of γ the edges of the shell are relatively under-stiffened, and hence the applicability of linear theory is in doubt. Therefore, the variation ratio $\gamma = 0.5$ seems preferable, even though for long shells $\gamma = 0.25$ yields higher structural efficiencies than $\gamma = 0.5$, (see Fig. 18).

3.4 COMPARISON BETWEEN THE GALERKIN METHOD AND THE METHOD OF "CORRECTING COEFFICIENTS"

The numerical results of the preceding sections were obtained by application of a Galerkin procedure to Eqs. (5). The stringer-stiffened axially compressed cylindrical shell is solved again by the method of "Correcting Coefficients", the details of which are given in the theoretical analysis. The results are compared to the more accurate ones obtained in the last section.

The expressions of Eqs. (31) were used for the correcting coefficients, with the implied assumption that the radial displacements at buckling have one half wave in the axial direction. This assumption is incorrect for low values of γ, where the "edge buckling" pattern dominates.

In Fig. 22 and Table 4, the ratio $P_{v.s}/P_{c.s}$, as obtained by the two different methods, is plotted versus Z for different values of γ. For $\gamma = 0.75$ the maximum difference amounts to less than 1%; but for $\gamma = 0.5$ it is 6%.

In general, the smaller γ the larger the differences. Typical cases computed with $\gamma = 0$

showed differences of more than 100%. The discrepancies result from a poor choice of the correcting coefficients. A better approximation (which was not used in the present work) employs Eqs. (32) for computation of the coefficients. Mathematically speaking, the method of "correcting coefficients" has no rigorous proof of convergence. It is based on physical and intuitive arguments. In [15] where the method was used for the first time, the results were not compared to those of a more rigorous solution. An approximate evaluation of their accuracy is obtained from the results of the present solution.

The main features of the method are:

a) reduction of the order of stability determinant of Eq. (17),

b) quicker convergence for the same number of terms in series (27) than the more accurate solution,

c) the values of the loads it yields are non-conservative,

d) its accuracy depends to a large extent on the choice of the correcting coefficients.

3.5. CYLINDRICAL SHELL UNDER HYDROSTATIC PRESSURE AND STIFFENED WITH UNIFORM STRINGERS AND RINGS OF NON-UNIFORM HEIGHT.

Uniformly ring-stiffened shells under hydrostatic pressure may buckle in one of two possible shapes, see [1]. For short shells, $Z < 1000$, and relatively heavy stiffeners, the $n \neq 1$ buckling shape is dominant reducing the efficiency of rings drastically. In [10] stringers were combined with rings to improve the structural efficiency. It was shown there that longitudinal stiffeners of cross sectional area amounting to only 5–10% of that of the rings, increase the buckling load of the shell by 50–70%. Further increase in the stringer area (with corresponding smaller rings) reduced the buckling pressure, because once the $n = 1$ mode of instability is dominant, rings are the best stiffeners.

The present analysis combines uniform stringers with rings of non-uniform height. The uniformity of the stringers simplifies the expressions of the integrals (16), reducing thereby the order of stability matrix, Eq. (17). Further details are given in Appendix F.

Fig. 23 and Table 5 analyse the influence of sinusoidal height variation of rings on the critical hydrostatic pressure. For values of Z below 1000, negative gains are obtained. These losses in efficiency may be attributed to the two main causes:

a) For short shells, $Z < 1000$, uniformly stiffened shells buckle in an $n \neq 1$ deflection shape. With non-uniform rings, the overstiffening of the middle of the shell, at the expense of the edges, causes,

therefore, large losses of efficiency in this range of Z.

b) For lateral pressure, an "edge buckling" pattern dominates for certain values of γ and shell geometry. A similar effect occurs in the case of hydrostatic pressure loading, and reduces the efficiency of non uniform stiffening.

These effects will henceforth be referred to as the "first" and "second" effect.

For short shells with Z below 100, Fig. 23, the first effect dominates, and there is practically no gain in load. For longer shells the curves go through a minimum whose magnitude depends primarily on the second effect. The lower the γ the larger the inefficiency of non-uniformed stiffening. Note that the curves to the right of the discontinuities in slope in Fig. 23, represent $n = 1$ buckling shapes. The magnitude of the gain is then similar to that obtained for lateral loading, Fig. 12. In order to explore possible improvements in the structural efficiency of shells (for stability), different combinations of stringers and rings (of constant weight) were analysed. The results are presented in Fig. 24 for a variation ratio $\gamma = 0.5$. Results for other values of γ are given in Table 5. Each curve in Fig. 24 has two discontinuities in slope. The intermediate range of Z, for which the $n \neq 1$ buckling shape dominates, decreases gradually with increasing stringer area. For large values of Z all curves merge into one.

If one aims at structural optimization, one must remember that increase of stringer area beyond a certain limit is detrimental to the efficiency of the stiffeners. The values of $(\lambda_p)_{cs}$ for different stiffener configurations are compared in Table 5 for a typical long shell (L/R=2, R/h=1000). A reduction of 25% in buckling load is found. For shorter shells an increase appears instead, but it gradually changes its sign to a reduction with increase in stringer area. Hence an optimum value of stringer area exists for every shell and ring geometry. Comparison of Fig. 25 with Fig. 24 brings out the influence of eccentricity of rings. The comparison shows that with outside rings, stringers of smaller cross-sectional area are needed. A similar behavior was already noticed in Fig. 12, where outside rings were also found to be better.

For hydrostatic pressure loading, both the symmetric and anti-symmetric components of the stability matrix, Eq. 17, have to be checked carefully. Axisymmetric buckling may occur for short shells with outside rings (see Table 5). Finally, one should remember to check the curve of load versus number of circumferential waves (t) in each case for a double minimum (see Fig. 9).

APPENDIX - A

THE GEOMETRICAL PARAMETERS OF THE STIFFENERS

Explicit expressions for the geometrical parameters of the stiffeners are given below, first for a general stiffener cross-section and then for stiffeners of rectangular cross-section. The distance between stiffeners is assumed to be uniform.

Parameter	*General Definition*	*Rectangular Cross Section*
$\mu_1^*(x)$	$(1-\nu^2)\,A_1(x)/bh$	$(1-\nu^2)\,[c_1(x)/h]\,[d_1(x)/b]$
$\mu_2^*(x)$	$(1-\nu^2)\,A_2(x)/ah$	$(1-\nu^2)\,[c_2(x)/h]\,[d_2(x)/a]$
$\chi_1^*(x)$	$\mu_1^*(x)\,e_1(x)/R$	$\mu_1^*(x)\,\{[c_1(x)+h]/2R\}\,\epsilon$
$\chi_2^*(x)$	$\mu_2^*(x)\,e_2(x)/R$	$\mu_2^*(x)\,\{[c_2(x)+h]/2R\}\,\epsilon$
$\zeta_1^*(x)$	$12(R/h)^2\,\chi_1^*(x)$	
$\zeta_2^*(x)$	$12(R/h)^2\,\chi_2^*(x)$	
$\eta_{01}^*(x)$	$12(1-\nu^2)\,I_{01}(x)/bh^3$	$12\mu_1^*(x)\{\frac{1}{12}[\frac{c_1(x)}{h}]^2+\frac{1}{4}[1+\frac{c_1(x)}{h}]^2\}$
$\eta_{02}^*(x)$	$12(1-\nu^2)\,I_{02}(x)/ah^3$	$12\mu_2^*(x)\{\frac{1}{12}[\frac{c_2(x)}{h}]^2+\frac{1}{4}[1+\frac{c_2(x)}{h}]^2\}$
$\eta_{t1}^*(x)$	$12(1-\nu^2)\,GI_{t1}/Ebh^3$	$[2/(1+\nu)]\,\mu_1^*(x)\,[(d_1(x)/b)\,(b/h)]^2$
$\eta_{t2}^*(x)$	$12(1-\nu^2)\,GI_{t2}/Ebh^3$	$[2/(1+\nu)]\,\mu_2^*(x)\,[(d_2(x)/a)\,(a/h)]^2$

where

$$\epsilon = \begin{cases} 1 & \text{for inside stiffeners} \\ -1 & \text{for outside stiffeners} \end{cases}$$

Note that in the last two expressions, the torsion constant of a rectangular cross-section is computed with the assumption of $c/d \geq 3$. Hence $I_{t1}(x) = [c_1(x)\,d_1^3(x)]/3$.

APPENDIX – B

THE INTEGRALS $I_j(n,m)$ AND $K_j(n,m)$ FOR NON-UNIFORM STIFFENERS WITH A DISCONTINUITY IN SLOPE (see Fig. 26).

Evaluation of integrals (16) by bisection of the limits of integration is incorrect. The separation must be carried out from Eq. (5), by an analysis of two sets of differential equations for the different domains.

Another approach to the problem uses the expression of the virtual work instead of Eq. (1).

$$\delta U = \int_0^{2\pi} \int_0^{(L/R)} [N_x \delta\epsilon_x + N_\phi \delta\epsilon_\phi + N_{x\phi} \delta\gamma_{x\phi} - (M_x/R)(\delta\kappa_x) - (M_\phi/R)(\delta\kappa_\phi) + \\ + (M_{x\phi}/R)(\delta\kappa_{x\phi}) - (M_{\phi x}/R)(\delta\kappa_{x\phi}) + N_{x0}\,\delta\epsilon'_x + N_{\phi 0}\,\delta\epsilon'_\phi]\, R^2\, dx\, d\phi = 0 \qquad (B-1)$$

It should be noted that neither the forces nor the moments in Eq. (B.1) are differentiated with respect to x.

Now ϵ'_x and ϵ'_ϕ are non-linear strains defined by

$$\epsilon'_x = (w^2_{,x}/2) \qquad \epsilon'_\phi = (w^2_{,\phi}/2) \qquad (B-2)$$

Substitution of the expression for the strains and curvatures, Eqs. (4) and (B.2), into (B.1) yields

$$\delta v = \int_0^{2\pi} \int_0^{L/R} [N_x (\delta u)_{,x} + N_\phi \delta(v_{,\phi} - w) + N_{x\phi} \delta(v_{,x} + u_{,\phi}) - (M_x/R)(\delta w)_{,xx} - \\ - (M_\phi/R)(\delta w)_{,\phi\phi} + (M_{x\phi}/R)(\delta w)_{,x\phi} + N_{x0}\, w_{,x}\, (\delta w)_{,x} + N_{\phi 0}\, w_{,\phi}\, (\delta w)_{,\phi}](R^2\, dx\, d\phi) = 0 \qquad (B-3)$$

Integration by parts of Eq. (B.3) yields the equilibrium equations, Eqs. (1), and the boundary conditions Eqs. (7).

Displacements and permissible variations are assumed as in Eqs. (9) and (10). The differentiation and integration performed is shown on a typical term of Eq. (B.3).

$$-\int_0^{2\pi}\int_0^{(L/R)} (M_x/R)(\delta w)_{,xx}\,dx\,d\phi = (D/R^2)\int_0^{2\pi}\int_0^{(L/R)} \{w_{,xx}[1+\eta_{01}^*(x)] + \nu w_{,\phi\phi} - u_{,x}\zeta_1^*(x)\}(\delta w)_{,xx}\,dx\,d\phi =$$

$$= -(D/R^2)\sum_{n=1}^{\infty}\Big\{\delta C_m (m\beta)^2 \int_0^{2\pi}\sin^2 t\phi\,d\phi \int_0^{L/R}\{-C_n n^2\beta^2 \sin n\beta x \cdot$$

$$\cdot [1+\eta_{01}^*(x)] - C_n \nu t^2 \sin n\beta x + A_n n\beta \sin n\beta x\, \zeta_1^*(x)\}\sin m\beta x\,dx\Big\} =$$

$$= (D/R^2)(\pi^2/2\beta)\sum_{n=1}^{\infty}\Big\{\delta C_m\{C_n[(n^4\beta^4 + \nu t^2 n^2\beta^2)\delta_{nm} + \qquad \text{(B-4)}$$

$$+ C_n n^2 m^2 \beta^4 I_3(n,m) - A_n n m^2 \beta^3 12(R/h)^2 I_2(n,m)\}\Big\}$$

where

$$I_2(n,m) = [1/12(R/h)^2](2\beta/\pi)\int_0^{(L/R)} \zeta_1^*(x)\sin n\beta x \sin m\beta\,dx$$
$$\text{(B-5)}$$
$$I_3(n,m) = (2\beta/\pi)\int_0^{(L/R)} \eta_{01}^*(x)\sin n\beta x \sin m\beta x\,dx$$

The variation of the geometrical parameters of the stiffeners is assumed to be symmetric with respect to $x = (L/2R)$ (see Fig. 26).

$$\eta_{01}^*(x) = \eta_{01}^*[(L/R) - x] \qquad \zeta_1^*(x) = \zeta_1^*[(L/R) - x] \qquad \text{(B-6)}$$

Bisection of the limits of integration in Eqs. (B.5) and use of (B.6) yields

$$I_3(n,m) = (2\beta/\pi)\Big\{\int_0^{(L/R)} \eta_{01}^*(x)\sin n\beta x \sin m\beta x\,dx + \int_{(L/2R)}^{(L/R)} \eta_{01}^*[(L/R)-x]\sin n\beta x \sin m\beta x\,dx\Big\} \qquad \text{(B-7)}$$

In the second integral the variable x is replaced by $y = (L/R) - x$

$$\int_{(L/2R)}^{(L/R)} \eta_{01}^*[(L/R)-x]\sin n\beta x \sin m\beta x\,dx = \int_0^{(L/2R)} \eta_{01}^*(y)\sin(n\pi - ny\beta)\sin(m\pi - my\beta)\,dy$$
$$\text{(B-8)}$$
$$= (-1)^{n+m}\int_0^{(L/2R)} \eta_{01}^*(y)\sin n\beta y \sin m\beta y\,dy$$

Substitution of Eq. (B.8) back into Eq. (B.7) yields

$$I_3(n,m) = (2\beta/\pi)[1 + (-1)^{n+m}]\int_0^{(L/2R)} \eta_{01}^*(x)\sin n\beta x \sin m\beta x\,dx \qquad \text{(B-9)}$$

The expression for $I_2(n,m)$ can be worked out in a similar manner as

$$I_2(n,m) = (2\beta/\pi)\left[1 + (-1)^{n+m}\right] \int_0^{(L/2R)} \chi_1^*(x) \sin n\beta x \sin m\beta x \, dx \qquad (B-10)$$

The other integrals of Eq. (16) are evaluated from the variational expression, Eq. (B. 8), in a similar manner.

APPENDIX - C

SOLUTION OF STABILITY DETERMINANT.

Application of Gauss's algorithm to the system of equations (17) yields

$$\begin{bmatrix} \triangledown F_A^* & F_B^* & F_C^* \\ 0 & \triangledown G_B^* & G_C^* \\ 0 & 0 & M-N\psi \end{bmatrix} \begin{Bmatrix} A_n \\ B_n \\ C_n \end{Bmatrix} = \{0\} \qquad (C-1)$$

where $\triangledown$ is the symbol for an upper triangular matrix

N is a diagonal matrix

ψ is an eigen-value

The last N equations uncouple, yielding

$$[M]\{C_n\} = \psi[N]\{C_n\} \qquad (C-2)$$

premultiplication by M^{-1} yields

$$(1/\psi)\{C_n\} = [M^{-1}][N]\{C_n\} = [\bar{M}]\{C_n\} \qquad (C-3)$$

$[M]$ is a non-singular matrix, as otherwise $\psi = 0$ is an eigen-value ($\psi = 0$ means zero buckling load).

$\bar{M}$ is not symmetric. It is, however, of the type called "symmetrisable", since the original matrices $[M]$ and $[N]$ are symmetric and $[N]$ is positive definite, see [20]. The eigen-values of $\bar{M}$ are therefore all real. The lowest one is obtained by the basic technique of matrix iteration. The convergence is accelerated by exponential extrapolation.

It should be mentioned that the proposed method for solving the stability determinant (17) is quick and precise. For a digital computer working with simple precision, 6 digits accuracy was obtained for matrices of order 100.

APPENDIX - D

NON-UNIFORM RING STIFFENERS

D.1 REDUCTION OF THE ORDER OF STABILITY DETERMINANT

If only rings are used as stiffeners,

$$\mu_1^*(x) = \eta_{01}^*(x) = \chi_1^*(x) = \eta_{t1}^*(x) = 0 \tag{D.1}$$

The torsional stiffness of the rings is neglected here, and therefore (see Eqs. (16))

$$I_j(n,m) = 0 \qquad j = 1, 2, 3, 4 \tag{D.2}$$

The matrices $[F_A]$ $[F_B]$ and $[F_C]$ degenerate into diagonal ones, see Eqs. (12), thereby permitting simultaneous solution of the first N equations of the stability matrix, Eq. (17). Hence

$$F_A(n,m)\, A_n + F_B(n,m)\, B_n + F_C(n,m)\, C_n = 0$$

and

$$A_n = -\frac{F_B(n,m)}{F_A(n,m)} B_n - \frac{F_C(n,m)}{F_A(n,m)} C_n \tag{D.3}$$

The coefficients of the remaining 2N equations, in Eq. (17), are reorganized in the form:

$$\sum_n [\bar{G}_B(n,m)\, B_n + \bar{G}_C(n,m)\, C_n] = 0$$

$$\sum_n [\bar{H}_B(n,m)\, B_n + \bar{H}_C(n,m)\, C_n] = 0 \qquad n, m = \begin{cases} 1, 3 \ldots \\ 2, 4 \ldots \end{cases} \tag{D.4}$$

$$\bar{G}_B(n,m) = \frac{[(1-\nu)/2]\,(t^2 + n^2\beta^2)^2}{n^2\beta^2 + [(1-\nu)/2]t^2}\,\delta_{nm} + t^2 K_1(n,m)$$

$$\bar{G}_C(n,m) = \bar{H}_B(n,m) = \left\{1 - \frac{\nu[(1+\nu)/2]\, n^2\beta^2}{n^2\beta^2 + [(1-\nu/2]t^2}\right\} t\,\delta_{nm} + t K_1(n,m) - t^3 K_2(n,m) \tag{D.5}$$

$$\bar{H}_C(n,m) = \left[1 - \frac{(\nu n\beta)^2}{n^2\beta^2 + [(1-\nu)/2]t^2} + \frac{(n^2\beta^2+t^2)^2}{12(R/h)^2} - \frac{\lambda_p t^2}{12(R/h)^2}\right]\delta_{nm} + K_1(n,m)$$

$$- 2t^2 K_2(n,m) + \frac{t^4 K_3(n,m)}{12(R/h)^2} \qquad (D.5)$$

Note that here the applied load is lateral pressure.

D.2 FORMULATION OF INTEGRALS $K_j(n,m)$ FOR RINGS WITH SINUSOIDAL HEIGHT VARIATION

The variation of the height of the rings along the generator is assumed to obey the law

$$c_2(x) = c_2^* \sin \beta x + c_{02} \qquad (D.6)$$

where c_{02} is the height of a uniform ring distribution, and c_2^* is the maximum height of the non-uniform part.

Sinusoidal variation is analysed since both stiffened and unstiffened shells buckle under lateral pressure with one half sine wave along the generator.

The non-uniform rings, Eq. (D.6), are compared to uniform ones of the same weight. If the width of the rings is the same in both cases the equivalent height is

$$\bar{c}_2 = c_{02} + c_2^* 2/\pi \qquad (D.7)$$

The "variation ratio", γ, is defined by

$$\gamma = c_{,2}/\bar{c}_2 \qquad (D.8)$$

Substitution of (D.7) and (D.8) into (D.6) yields

$$c_2(x) = \bar{c}_2[\gamma + (\pi/2)(1-\gamma)\sin \beta x] \qquad (D.9)$$

The geometrical parameters of the rings $\mu_2^*(x)$, $\chi_2^*(x)$ and $\eta_{02}^*(x)$ are defined for rectangular cross-sections in Appendix A. Substitution of Eq. (D.9) into those definitions yields

$$\mu_2^*(x) = (1-\nu^2)(d_2/a)\, a_1 (\alpha + \sin \beta x)$$

$$\chi_2^*(x) = \epsilon[(1-\nu^2)/2(R/h)]\,(d_2/a)\, a_1\, (\alpha + \sin\beta x)\,[1 + a_1 (\alpha + \sin \beta x)]$$

$$\eta_{02}^*(x) = 12(1-\nu^2)(d_2/a)\, a_1 \left\{[[a_1^2 (\alpha+\sin\beta x)^3]/12] + [(\alpha+\sin\beta x)/4]\,[1+a_1(\alpha+\sin\beta x)]^2\right\} \qquad \text{(D. 10)}$$

where

$$a_1 = (1-\gamma)\,(\pi/2)\,(\bar{c}_2/h)$$

and (D. 11)

$$\alpha = (2\gamma/\pi)/(1-\gamma)$$

The integrals $K_j(n,m)$, Eqs. (16), are now computed with aid of Eqs. (D. 10) and yield

$$K_1(n,m) = (1-\nu^2)(d_2/a)\, a_1\, [\alpha \delta_{nm} + L_1(n,m)]$$

$$K_2(n,m) = \epsilon[(1-\nu^2)/2(R/h)](d_2/a)\, a_1 \{[\alpha + \alpha^2 a_1 + (a_1/2)]\,\delta_{nm} + (1+2\alpha a_1)\, L_1(n,m) -$$

$$-(a_1/4)(\delta_{|n,m|,2} - \delta_{1,1})\}$$

$$K_3(n,m) = 12(1-\nu^2)(d_2/a)\, a_1 \left\{[(\alpha^3 a_1^2/3) + (\alpha+a_1)(1+2\alpha a_1)/4]\,\delta_{nm} + \{[(1+2\alpha a_1)^2 + a_1^2]/4\}\, L_1(n,m) -\right.$$

$$\left. -(a_1/8)(1+2\alpha a_1)\,(\delta_{|n-m|,2} - \delta_{1,1}) - (a_1^2/12)\, L_2(n,m)\right\} \qquad \text{(D. 12)}$$

where

$$\delta_{1,1} = \begin{cases} 1 & n = m = 1 \\ 0 & n \neq 1 \text{ or } m \neq 1 \end{cases} \qquad \text{and} \qquad \delta_{|m-n|,2} = \begin{cases} 1 & |n-m| = 2 \\ 0 & |n-m| \neq 2 \end{cases}$$

$$L_1(n,m) = \frac{[1+(-1)^{n+m}]}{\pi}\left[\frac{1}{1-(n-m)^2} - \frac{1}{1-(n+m)^2}\right]$$

$$L_2(n,m) = \frac{3[1+(-1)^{n+m}]}{\pi}\left[\frac{1}{9-(n-m)^2} - \frac{1}{9-(n+m)^2}\right] \qquad \text{(D. 13)}$$

Note that $L_1(n,m)$ and $L_3(n,m)$ are zero for odd values of $/n-m/$

D.3 FORMULATION OF INTEGRALS $K_j(n,m)$ FOR RINGS WITH SINUSOIDAL WIDTH VARIATION

The height of the rings is uniform along the shell while the width varies according to

$$d_2(x) = d_2^* \sin \beta x \tag{D.14}$$

The ring height distribution given by (D.14) does not include a uniform part along the generator. The equivalent width is now

$$\bar{d}_2 = d_2^* 2/\pi$$

Therefore

$$d_2(x) = (\pi/2)\,\bar{d}_2 \sin \beta x \tag{D.15}$$

Substitution of Eq. (D.15) in the definitions of μ_2^*, η_{02}^* and χ_2^* yields

$$\begin{aligned}
\mu_2^*(x) &= (1-\nu^2)(c_2/h)(\bar{d}_2/a)(\pi/2)\sin \beta x \\
\chi_2^*(x) &= \epsilon[(1-\nu^2)/2(R/h)](c_2/h)(\bar{d}_2/a)[(c_2/h)+1](\pi/2)\sin \beta x \\
\eta_{02}^*(x) &= 12(1-\nu^2)(c_2/h)(\bar{d}_2/a)\{[(c_2/h)^2/12] + [[(c_2/h)+1]/2]^2\}(\pi/2)\sin \beta x
\end{aligned} \tag{D.16}$$

The expression for the integrals, Eqs. (16), is

$$\begin{aligned}
K_1(n,m) &= (1-\nu^2)(c_2/h)(\bar{d}_2/a)\,L_1(n,m) \\
K_2(n,m) &= [\epsilon(1-\nu^2)/2(R/h)](c_2/h)(\bar{d}_2/a)[(c_2/h)+1]\,L_1(n,m) \\
K_3(n,m) &= 12(1-\nu^2)(c_2/h)(\bar{d}_2/a)\{[(c_2/h)^2/12] + [[c_2(h+1)]/2]^2\}\,L_1(n,m)
\end{aligned} \tag{D.17}$$

$$L_1(n,m) = \frac{[1+(-1)^{n+m}]}{2}\left[\frac{1}{1-(n-m)^2} - \frac{1}{1-(n+m)^2}\right]$$

APPENDIX - E

NON-UNIFORM STRINGERS

E.1 REDUCTION OF THE ORDER OF STABILITY DETERMINANT

For stringers only

$$\mu_2^*(x) = \chi_2^*(x) = \eta_{02}^*(x) = \eta_{t2}^*(x) = 0 \tag{E.1}$$

and therefore (see Eqs. 16)

$$K_j(n,m) = 0 \qquad j = 1, 2, 3 \tag{E.2}$$

Matrices $[G_A]$, $[G_B]$ and $[G_C]$ degenerate to diagonal ones, see Eqs. 13. The second set of Eqs. (11) is solved simultaneously

$$B_n = -\frac{G_A(n,m)}{G_B(n,m)} A_n - \frac{G_C(n,m)}{G_B(n,m)} C_n \tag{E.3}$$

The new coefficients of the starility determinant of Eq. (17), are

$$\begin{aligned} \sum_n [\bar{\bar{F}}_A(n,m) A_n + \bar{\bar{F}}_C(n,m) C_n] &= 0 \\ \sum_n [\bar{\bar{H}}_A(n,m) A_n + \bar{\bar{H}}_C(n,m) C_n] &= 0 \end{aligned} \tag{E.4}$$

where

$$\bar{\bar{F}}_A(n,m) = \frac{[(1-\nu)/2](n^2\beta^2 + t^2)^2}{t^2 + [(1-\nu)/2] n^2 \beta^2} \delta_{nm} + nm\beta^2 I_1(n,m)$$

$$\bar{\bar{F}}_C(n,m) = \bar{\bar{H}}_A(m,n) = \frac{[(1-\nu)/2] n\beta(\nu n^2\beta^2 - t^2)}{t^2 + [(1-\nu)/2] n^2\beta^2} \delta_{nm} - n^2 m \beta^3 I_2(n,m)$$

$$\bar{\bar{H}}_C(n,m) = \left[\frac{(n^2\beta^2 + t^2)^2}{12(R/h)^2} + \frac{[(1-\nu)/2] n^2\beta^2}{t^2 + [(1-\nu)/2] n^2\beta^2} - \frac{(\lambda/2) n^2\beta^2}{12(R/h)^2} \right] \delta_{nm} + \tag{E.5}$$

$$+ \frac{n^2 m^2 \beta^4 I_3(n,m) + t^2 n m \beta^2 I_4(n,m)}{12(R/h)^2} \qquad (E.5)$$

The applied load is here axial compression.

E.2 FORMULATION OF INTEGRALS $I_j(n,m)$ FOR STRINGERS WITH SINUSOIDAL HEIGHT VARIATION.

The assumptions and the details of the analysis are similar to those presented in the second part of Appendix D for rings with sinusoidal height variation. The subscript "2" (for rings) is replaced by subscript "1" (for stringers), e.g.

$c_2 \rightarrow c_1$

$c_{02} \rightarrow c_{01}$

and the appropriate expressions are obtained.

The stringer distribution corresponding to the ring distribution of Eq. (D.9) is then

$$c_1(x) = \bar{c}_1 [\gamma + (1-\gamma)(\pi/2) \sin \beta x] \qquad (E.6)$$

where $\bar{c}_1$ is the equivalent height of stringers and γ is the variation ratio.

If one introduces the notations

$$a = 2\gamma/\pi(1-\gamma)$$

and $$(E.7)$$

$$a_1 \quad \{\bar{c}_1/h\}\,[\pi(1-\gamma)/2]$$

the geometrical parameters of the stringers defined in Appendix A, become

$$\mu_1^*(x) = (1-\nu^2)(d_1/b)\, a_1 (a + \sin \beta x)$$

$$\chi_1^*(x) = \epsilon[(1-\nu^2)/2(R/h)](d_1/b)\, a_1 (a+\sin \beta x)[1 + a_1(a+\sin \beta x)]$$

$$\eta_{01}^*(x) = 12(1-\nu^2)(d_1/b)\, a_1 \{(a_1^2/12)(a+\sin \beta x)^2 + (1/4)(a+\sin \beta x)[1+a_1(a+\sin \beta x)]^2\} \qquad (E.8)$$

$$\eta_{c1}^{*}(x) = 2(1-\nu)(d_1/h)^3 (h/b)\, a_1\, (\alpha+\sin\beta x) \qquad \text{(E. 8)}$$

Substitution of Eq. (E. 8) into Eqs. (16) yields the appropriate integrals

$$I_1(n,m) = (1-\nu^2)(d_1/b)\, a_1\, [\alpha\delta_{nm} + L_1(n,m)]$$

$$I_2(n,m) = \epsilon[(1-\nu^2)/2(R/h)](d_1/b)\, a_1\, \{[\alpha+\alpha^2 a_1 + (a_1/2)]\delta_{nm} + (1+2\alpha a_1) L_1(n,m) - (\alpha/4)(\delta_{|n-m|,2} - \delta_{1,1})\}$$

$$I_3(n,m) = 12(1-\nu^2)(d_1/b)\, a_1 \{[(1/3)\alpha^3 a_1^2 + (1/4)(\alpha+a_1)(1+2\alpha a_1)]\delta_{nm} +$$

$$+ \{(1/4)[(1+2\alpha a_1)^2 + a_1^2]\} L_1(n,m) - (1/8) a_1 (1+2\alpha a_1)[\delta_{|n-m|,2} - \delta_{1,1}] - (a_1^2/12) L_2(n,m)\}$$

$$I_4(n,m) = 2(1-\nu)(d_1/h)^3 (h/b)\, a_1\, [\alpha\delta_{nm} + L_3(n,m)] \qquad \text{(E. 9)}$$

$$L_1(n,m) = \frac{[1+(-1)^{n+m}]}{\pi}\left[\frac{1}{1-(n-m)^2} - \frac{1}{1-(n+m)^2}\right]$$

$$L_2(n,m) = \frac{3[1+(-1)^{n+m}]}{\pi}\left[\frac{1}{9-(n-m)^2} - \frac{1}{9-(n+m)^2}\right]$$

$$L_3(n,m) = \frac{[1+(-1)^{n+m}]}{\pi}\left[\frac{1}{1-(n-m)^2} - \frac{1}{1-(n+m)^2}\right] \qquad \text{(E. 10)}$$

E.3 FORMULATION OF INTEGRALS $I_j(n,m)$ FOR STRINGERS WITH LINEAR HEIGHT VARIATION

see Fig. 2.

$$c_1(x) = c_{01} + c_1^{*}(2\beta/\pi)x \qquad 0 \le x \le \pi/2\beta$$

$$c_1(x) = c_{01} + c_1^{*}[2-(2\beta/\pi)x] \qquad \pi/2\beta \le x \le \pi/\beta$$

$$\pi/\beta = L/R \qquad \text{(E. 11)}$$

The equivalent height of the stringers is

$$\bar{c}_1 = c_{01} + (c_1^{*}/2) \qquad \text{(E. 12)}$$

Substitution of Eq. (E. 12) into Eq. (E. 11) yields

$$c_1(x) = \bar{c}_1 [\gamma + 2(1-\gamma)(2\beta/\pi)x] \qquad 0 \le x \le \pi/2\beta$$

$$c_1(x) = \bar{c}_1 \{\gamma + 2(1-\gamma)[2-(2\beta/\pi)x]\} \qquad (\pi/2\beta) \le x \le (\pi/\beta) \qquad \text{(E. 13)}$$

where γ is the variation ratio, defined here by $\gamma = c_{01}/\bar{c}_1$

The geometrical parameters of the stringers, for $0 \le x \le \pi/2\beta$ are obtained from Eq. (E. 8) by (a) permutation of $\sin\beta x$ to $\sin(2\beta/\pi)x$ (b) use of new definitions for a and c_1, see Eq. (E. 7)

$$a = \gamma/2(1-\gamma)$$

$$a_1 = (\bar{c}_1/h)[2(1-\gamma)] \qquad \text{(E. 14)}$$

The explicit expressions for integrals (16) are then

$$I_1(n,m) = (1-\nu^2)(d_1/b)\, a_1 [a\delta_{nm} + \bar{L}_1(n,m)]$$

$$I_2(n,m) = \epsilon[(1-\nu^2)/2(R/h)](d_1/b)a_1[(a+a^2a_1)\delta_{nm} + (1+2aa_1)\bar{L}_1(n,m) +$$

$$+ a_1 \bar{L}_2(n,m)]$$

$$I_3(n,m) = 12(1-\nu^2)(d_1/b)\, a_1 \{a[(a^2a_1^2/3) + (1+2aa_1)/4]\delta_{nm} +$$

$$+ [(1+2aa_1)/2]^2 \bar{L}_1(n,m) + [a_1(1+2aa_1)]/2]\bar{L}_2(n,m) + (a_1^2/3)\bar{L}_3(n,m)\}$$

$$I_4(n,m) = 2(1-\nu)(d_1/h)^3 (h/b)\, a_1 [a\delta_{nm} + \bar{L}_4(n,m)] \qquad \text{(E. 15)}$$

where

	$n = m$	$n \neq m$
$\bar{L}_1(n,m)$	$\frac{1}{2} + \frac{[1-(-1)^n]}{(\pi n)^2}$	$\frac{4}{\pi^2}[1+(-1)^{n+m}]\left\{\frac{1-(-1)^{\frac{n+m}{2}}}{(m+n)^2} - \frac{1-(-1)^{\frac{m-n}{2}}}{(m-n)^2}\right\}$
$\bar{L}_2(n,m)$	$\frac{1}{3} - \frac{2(-1)^n}{(\pi n)^2}$	$\frac{8}{\pi^2}[1+(-1)^{m+n}]\left\{\frac{(-1)^{\frac{m+n}{2}}}{(m+n)^2} - \frac{(-1)^{\frac{m-n}{2}}}{(m-n)^2}\right\}$
$\bar{L}_3(n,m)$	$\frac{1}{4} - \frac{6[1-(-1)^n]}{(\pi n)^4} - \frac{3(-1)^n}{(\pi n)^2}$	$\frac{96}{\pi^2}[1+(-1)^{n+m}]\left\{\frac{1-(-1)^{\frac{m-n}{2}}}{(m-n)^4} - \frac{1-(-1)^{\frac{m+n}{2}}}{(m+n)^4}\right\} + \frac{3}{2}\bar{L}_2(n,m)$
$\bar{L}_4(n,m)$	$\frac{1}{2} - \frac{[1-(-1)^n]}{(\pi n)^2}$	$-\frac{4}{\pi^2}[1+(-1)^{n+m}]\left\{\frac{1-(-1)^{\frac{m+n}{2}}}{(m+n)^2} + \frac{1-(-1)^{\frac{m-n}{2}}}{(m-n)^2}\right\}$

(E. 16)

APPENDIX - F

COMBINATION OF UNIFORM STRINGERS WITH RINGS OF NON UNIFORM HEIGHT

For uniform stringers, the matrices of the integrals $I_j(n,m)$, Eqs. (16), and those whose elements are $F_A(n,m)$, $F_B(n,m)$ and $F_C(n,m)$, see Eqs. (12), degenerate into diagonal matrices. Solution of the first N equations of (17) and simplification of the remaining matrix yields

$$\begin{bmatrix} G'_B & G'_C \\ H'_B & H'_C \end{bmatrix} \begin{Bmatrix} B_n \\ C_n \end{Bmatrix} = 0 \qquad (F.1)$$

where

$$G'_B(n,m) = \frac{[(1-\nu)/2](t^2+n^2\beta^2)^2}{(1+\mu_1)n^2\beta^2+[(1-\nu)/2]t^2}\,\delta_{nm} + t^2 K_1(n,m)$$

$$G'_C(n,m) = H'_B(n,m) = \left[1 - \frac{[(1+\nu)/2]n^2\beta^2(\nu-\chi_1 n^2\beta^2)}{(1+\mu_1)n^2\beta^2+[(1-\nu)/2]t^2}\right] t\,\delta_{nm} + t K_1(n,m) - t^3 K_2(n,m)$$

$$H'_C(n,m) = \left[1 + \frac{(n^2\beta^2+t^2)^2 + \eta_{01} n^4\beta^4}{12(R/h)^2} - \frac{n^2\beta^2(\nu-\chi_1 n^2\beta^2)^2}{(1+\mu_1)n^2\beta^2+[(1-\nu)/2]t^2} - \right.$$

$$\left. - \frac{\lambda_2(t^2+n^2\beta^2/2)}{12(R/h)^2}\right]\delta_{nm} + K_1(n,m) - 2t^2 K_2(n,m) + \frac{t^4 K_3(n,m)}{12(R/h)^2} \qquad (F.2)$$

The applied load in these equations is hydrostatic pressure.

For rings with sinusoidal height variation the values of integrals $K_j(n,m)$ are similar to those given in the second section of Appendix D.

CONCLUSIONS

The general instability of cylindrical shells with non-uniform stiffeners was analysed for lateral and hydrostatic pressure and for axial compression. Height and width variations of rings and stringers were considered and considerable improvements in structural efficiency were obtained. When most of the stiffening is concentrated at the mid length of the shell, an edge type buckling mode may appear and reduce the structural efficiency drastically. Hence it was found advisable in many cases to supplement the varying part of the stiffener by a uniform part. The "variation ratio" γ characterizes the extent of the uniform supplement.

For lateral pressure loading, gains of 70–80% in general instability pressure are obtained with rings of non-uniform height at optimal values of γ. For prescribed loading conditions the gains result in 10–25% weight saving. Width variation is less efficient and rings of non-uniform width yield only 15–20% gains in load but the corresponding weight savings remain at 10–20%.

For axial compression, stringers with sinusoidal and linear height variation were studied. Sinusoidal variation is found to be superior to linear variation, and gains in buckling load of 30%, with corresponding weight savings of 10%, are obtained. A variation ratio $\gamma = 0.5$ appears to be roughly optimal.

For hydrostatic pressure loading, a combination of rings and stringers with a weight ratio 10 to 1, is found to be roughly optimal. Combinations of non-uniform rings and stringers under axial compression and hydrostatic pressure should be further investigated.

Comparison of solution by a straightforward Galerkin method and by the method of "correcting coefficients" indicates that in the relatively simple case investigated here, the loss in accuracy in the second method outweighs the numerical difficulties of the first.

REFERENCES

1. Singer, J., Baruch, M., and Harari, O., "Further Remarks on the Effect of Eccentricity of Stiffeners on the General Instability of Stiffened Cylindrical Shells", TAE Report 42, Technion Research and Development Foundation, Haifa, Israel, Aug. 1965. (To be published in the December 1966 issue of the Journal of Mech. Eng. Science.)

2. Baruch, M., Singer, J., and Weller, T., "Effect of Eccentricity of Stiffeners on the General Instability of Stiffened Cylindrical Shells under Torsion", Proceedings of the 8th Israel Annual Conference on Aviation and Astronautics, Israel Journal of Technology, 4, No. 1, 144-154, (1966). Also TAE Report 43, Technion Research and Development Foundation, Haifa, Israel, Aug. 1965.

3. Singer, J., Baruch, M., and Harari, O., "On the Stability of Eccentrically Stiffened Cylindrical Shells Under Axial Compression", TAE Report 44, Technion Research and Development Foundation, Haifa, Israel, December 1965.

4. Milligan, R., Gerard, G., Lakshmikantham, C., and Becker, H., "General Instability of Orthotropic Stiffened Cylinders", Report AFFDL-TR-65-161, Air Force Flight Dynamics Laboratory. USAF, Wright Patterson Air Force Base, Ohio, July 1965.

5. Katz, L., "Compression Tests on Integrally Stiffened Cylinders", NASA TMX-53315, August 1965.

6. Card, M.F., "Preliminary Results of Compression Tests on Cylinders with Eccentric Longitudinal Stiffeners", NASA TMX-1064, Sept. 1964.

7. Timoshenko, S.P., and Gere, J.M., "Theory of Elastic Stability", 2nd ed., p. 131, McGraw-Hill, New York, 1963.

8. Hertel, H., "Leichtbau", 1st ed., p. 205, Springer-Verlag, Berlin 1960.

9. Baruch, M., Singer, J., and Harari, O., "General Instability of Conical Shells with Non-Uniformly Spaced Stiffeners Under Hydrostatic Pressure", Proceedings of the 7th Israel Annual Conference on Aviation and Astronautics, Israel Journal of Technology, 3, No. 1, 62-71 (1965). Also TAE 37, Technion Research and Development Foundation, Haifa, Israel, December 1964.

10. Singer, J., and Baruch, M., "Recent Studies on Optimization for Elastic Stability of Cylindrical and Conical Shells", presented at the 5th I.C.A.S. Congress, London, September 1966.

11. Baruch, M., and Singer, J., "Effect of Eccentricity of Stiffeners on the General Instability of Stiffened Cylindrical Shells Under Hydrostatic Pressure", The Journal of Mech. Eng. Science 5, No. 1, 23-27, (1963).

12. Moe, J., "Stability of Rib-Reinforced Cylindrical Shells under Lateral Pressure", Publications Inter. Ass. Bridge Struc. Eng., 18, 113-136 (1958).

13. Block, D.L., "Influence of Ring Stiffeners on Instability of Orthotropic Cylinders in Axial Compression", NASA TN D 2482, October 1964.

14. Donnell, L.H., "Stability of Thin Walled Tubes Under Torsion", NACA Rep. 479, May 1933.

15. Baruch, M., and Singer, J., "General Instability of Stiffened Circular Conical Shells under Hydrostatic Pressure", The Aeronautical Quarterly, 26, 2, 187-204 (1965). Also TAE Report 28, Technion Research and Development Foundation, Haifa, Israel, June 1963.

16. Batdorf, S.B., "Simplified Method of Elastic Stability Analysis for Thin Cylindrical Shells", NACA Report 874, 1947.

17. Gerard, G., "Minimum Weight Design of Ring Stiffened Cylinders Under External Pressure", Journal of Ship Research, 5, 44-49, (1961).

18. Burns, A.B., and Almroth, B.O., "Structural Optimization of Axially Compressed Ring-Stringer Stiffened Cylinders", Journal of Spacecraft and Rockets, 3, No. 1, 19-25, (1966).

19. Gerard, G., "Elastic and Plastic Stability of Orthotropic Cylinders", Collected Papers on Instability of Shell Structures, NASA TN D 1510, pp. 277-295, December 1962.

20. Hildebrand, F.B., "Methods of Applied Mathematics", 1st ed., p. 7, Prentice-Hall, Englewood Cliffs, N.J., 1961.

ACKNOWLEDGEMENT

The authors would like to thank Miss A. Adler for assistance with the computations and the staff of the Technion Computing Center for their valuable help.

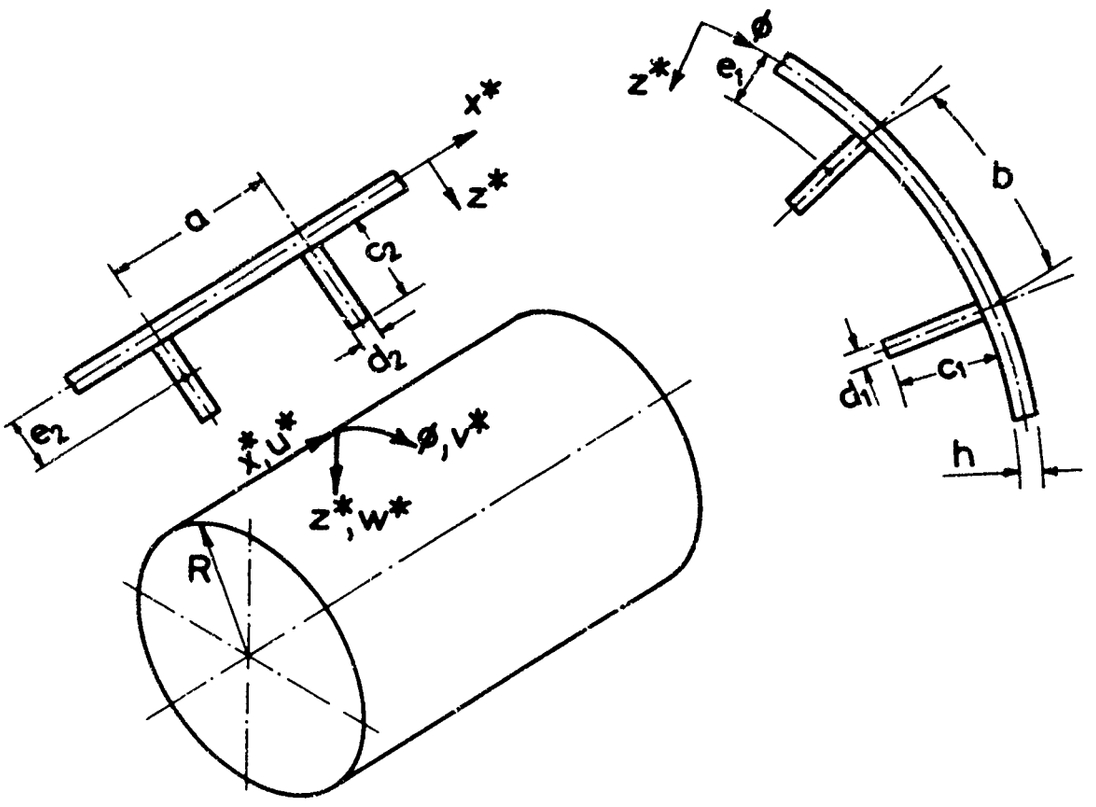

FIG. 1 NOTATION

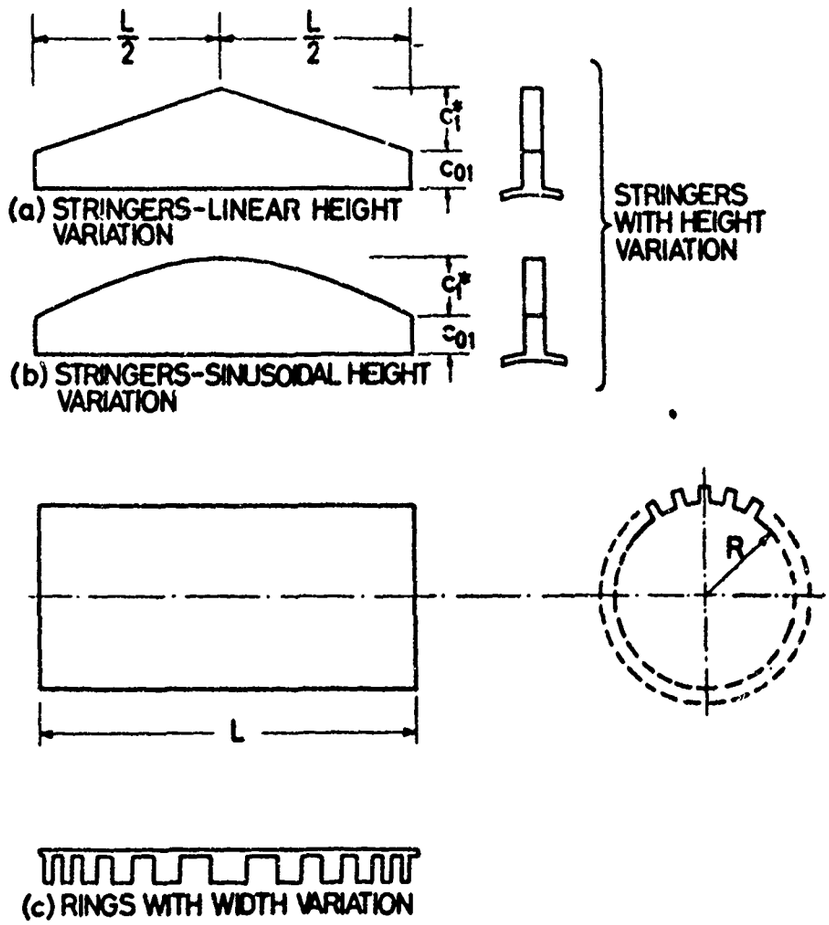

FIG. 2 TYPES OF STIFFENER AREA VARIATIONS

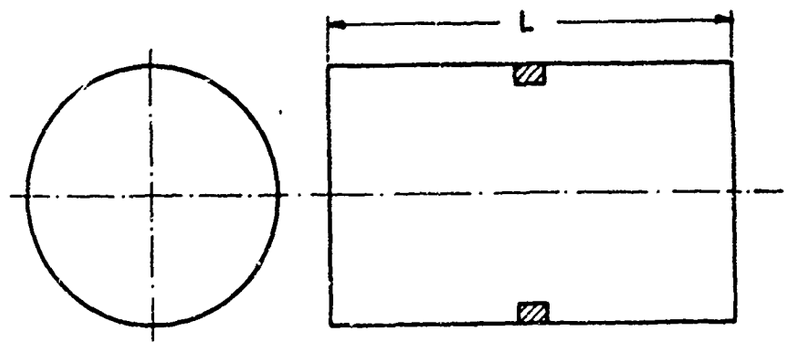

FIG. 3 SHELL WITH CENTRALLY CONCENTRATED RING

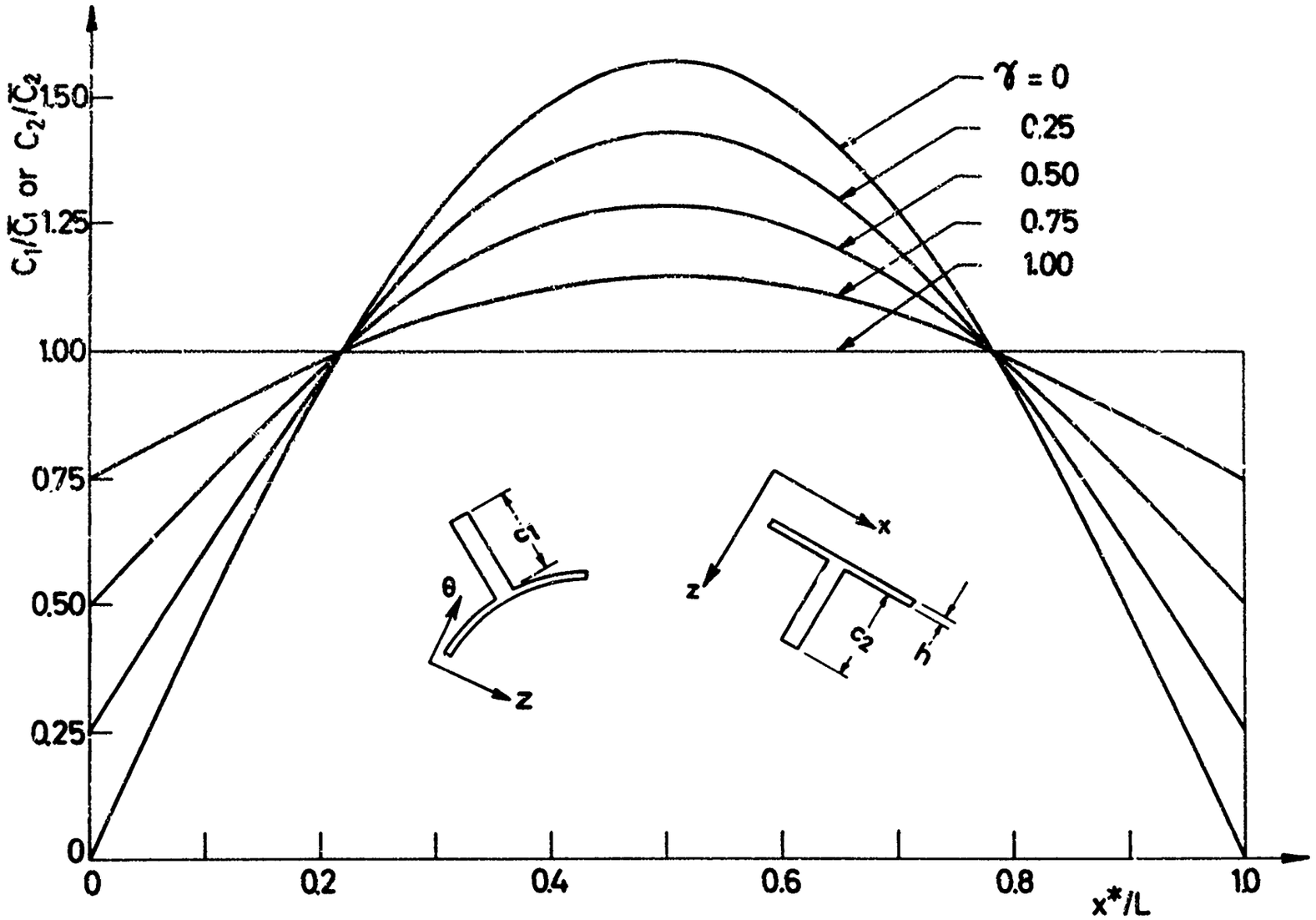

FIG. 4 HEIGHT VARIATION OF STIFFENERS FOR DIFFERENT VARIATION RATIOS

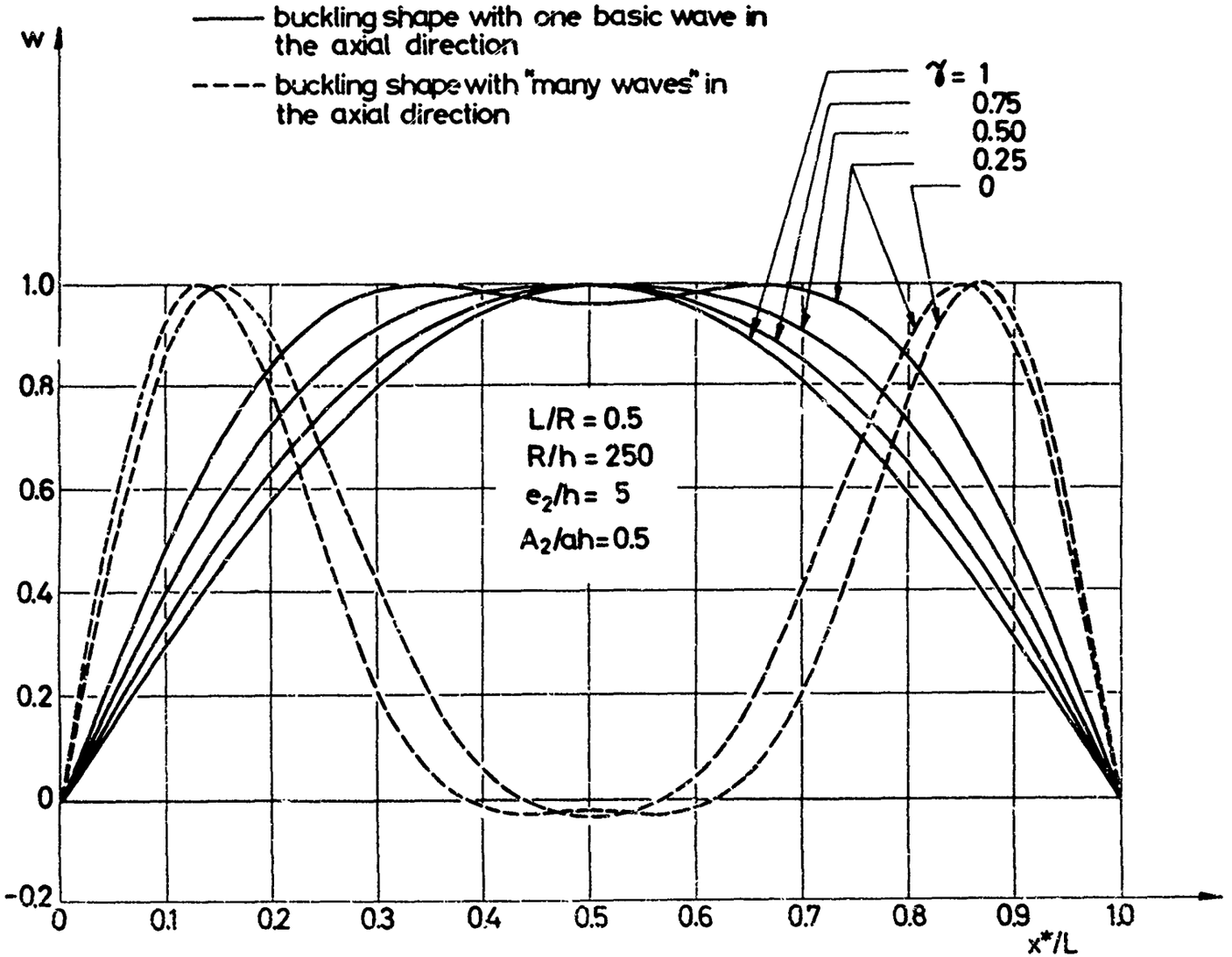

FIG. 5 DEFLECTION SHAPES FOR LATERALLY LOADED CYLINDRICAL SHELLS STIFFENED WITH INSIDE RINGS OF NON-UNIFORM HEIGHT

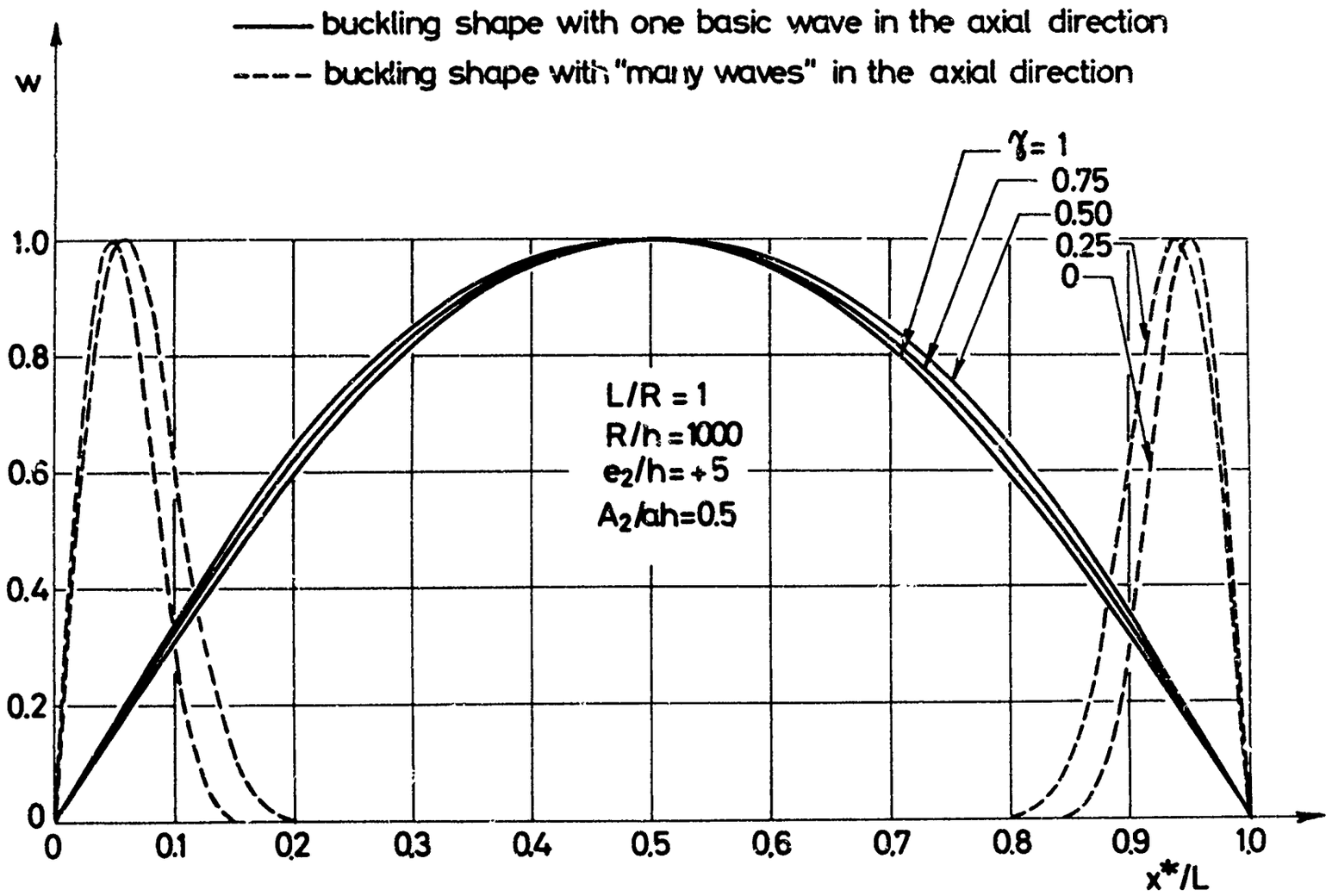

FIG. 6 DEFLECTION SHAPES FOR LATERALLY LOADED CYLINDRICAL SHELLS STIFFENED WITH INSIDE RINGS OF NON-UNIFORM HEIGHT

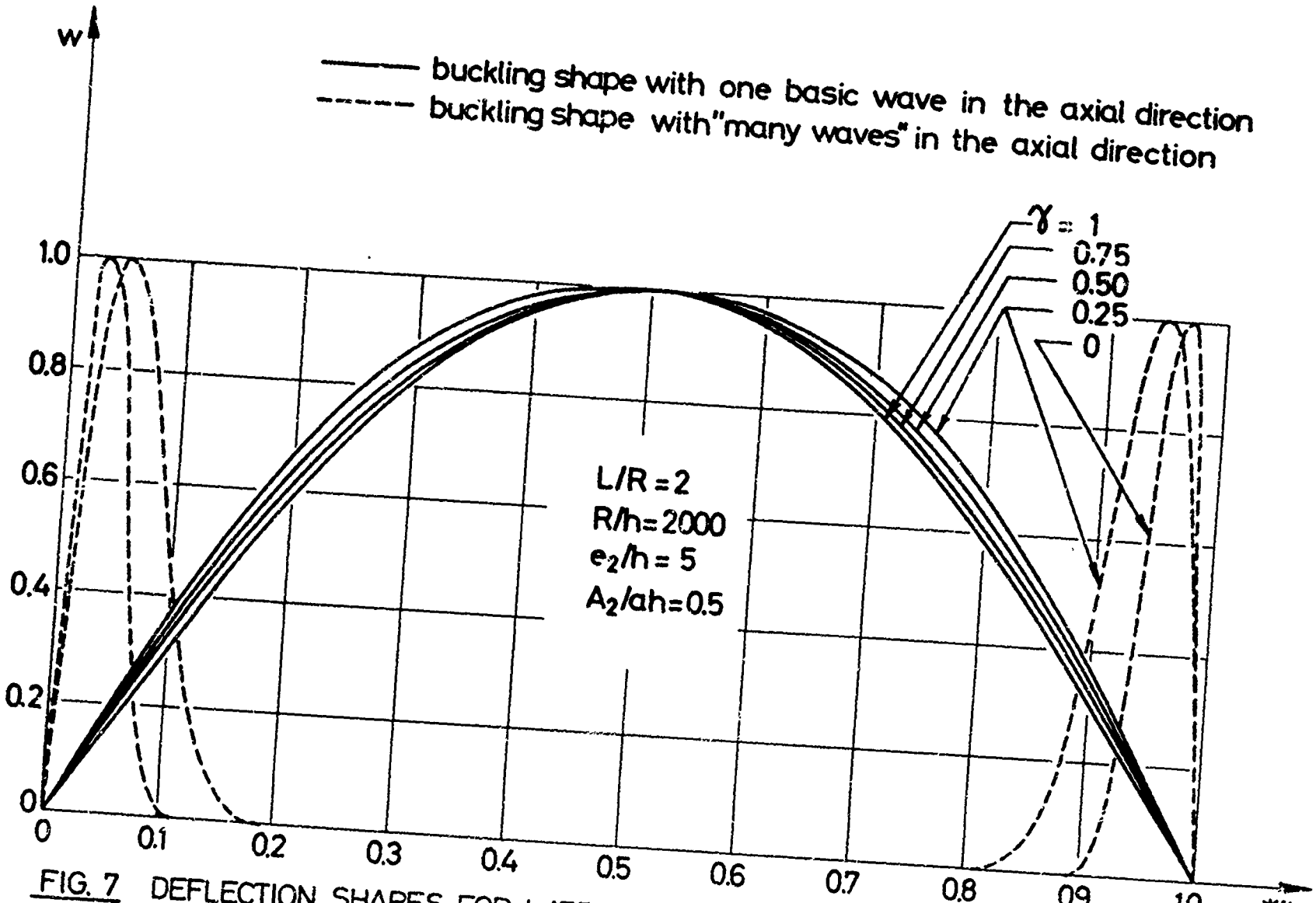

FIG. 7 DEFLECTION SHAPES FOR LATERALLY LOADED CYLINDRICAL SHELLS STIFFENED WITH INSIDE RINGS OF NON-UNIFORM HEIGHT

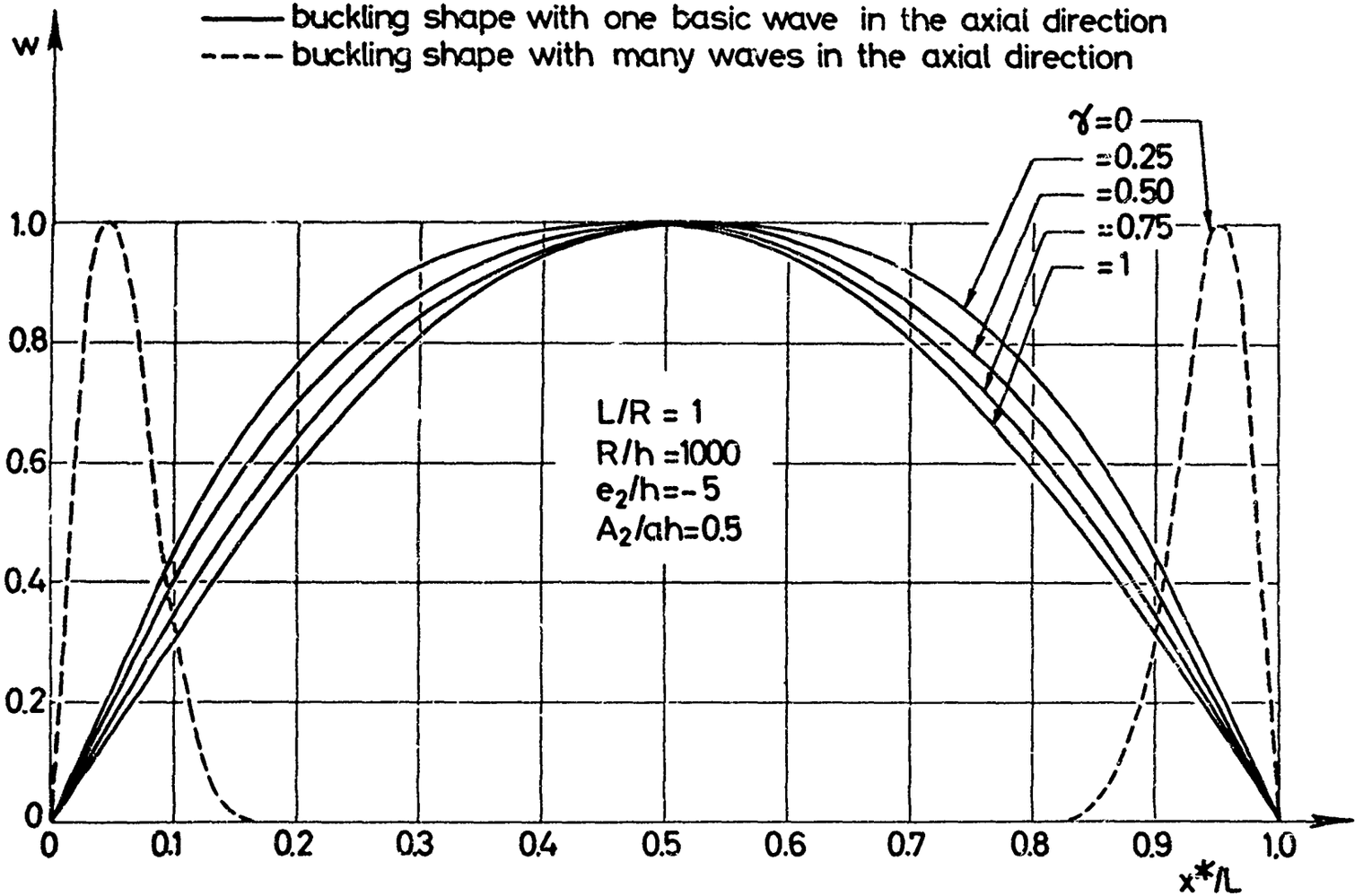

FIG. 8 DEFLECTION SHAPES FOR LATERALLY LOADED CYLINDRICAL SHELLS STIFFENED WITH OUTSIDE RINGS OF NON-UNIFORM HEIGHT

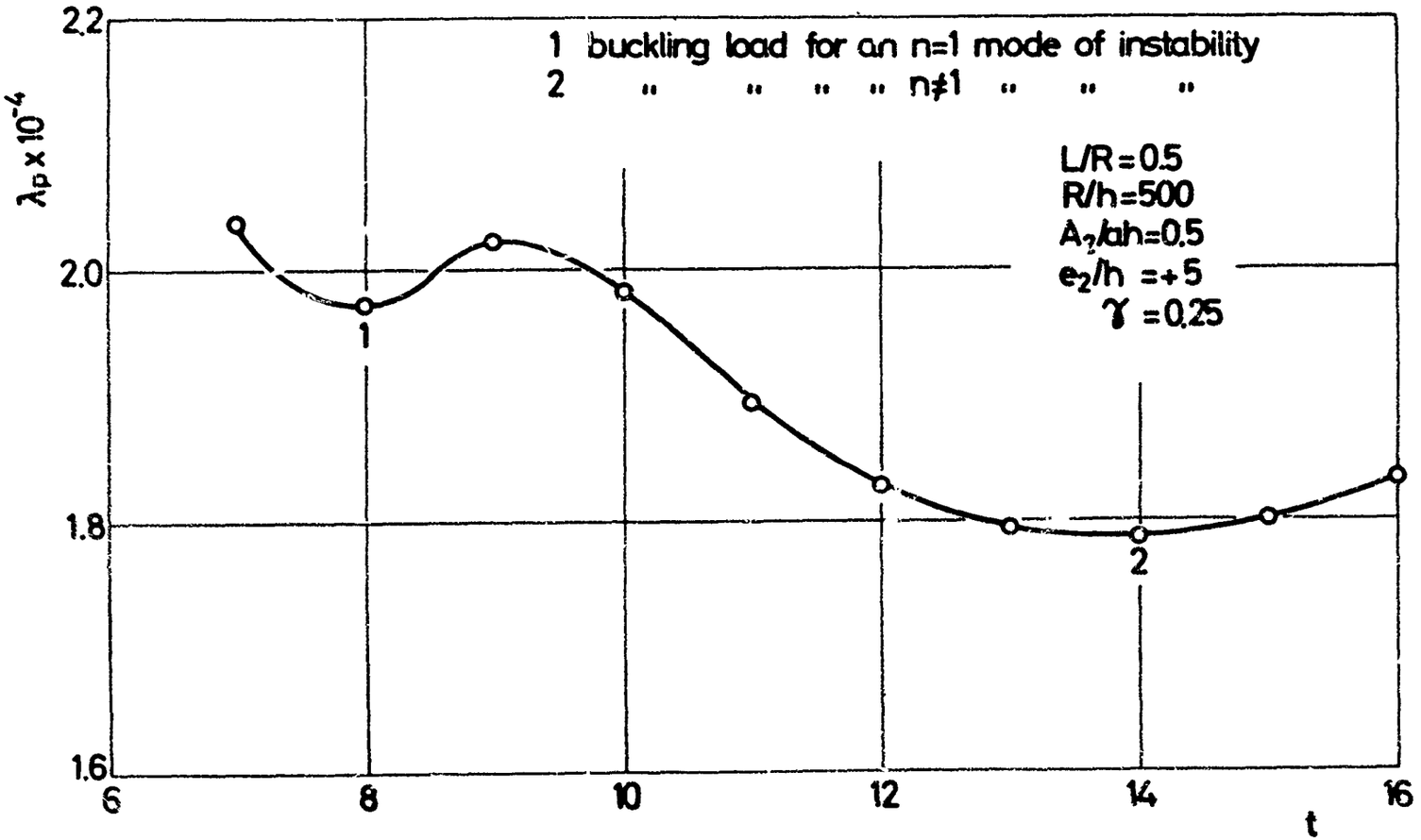

FIG. 9 TYPICAL CURVE OF PRESSURE PARAMETER VERSUS NUMBER OF CIRCUMFERENTIAL WAVES (LATERAL PRESSURE)

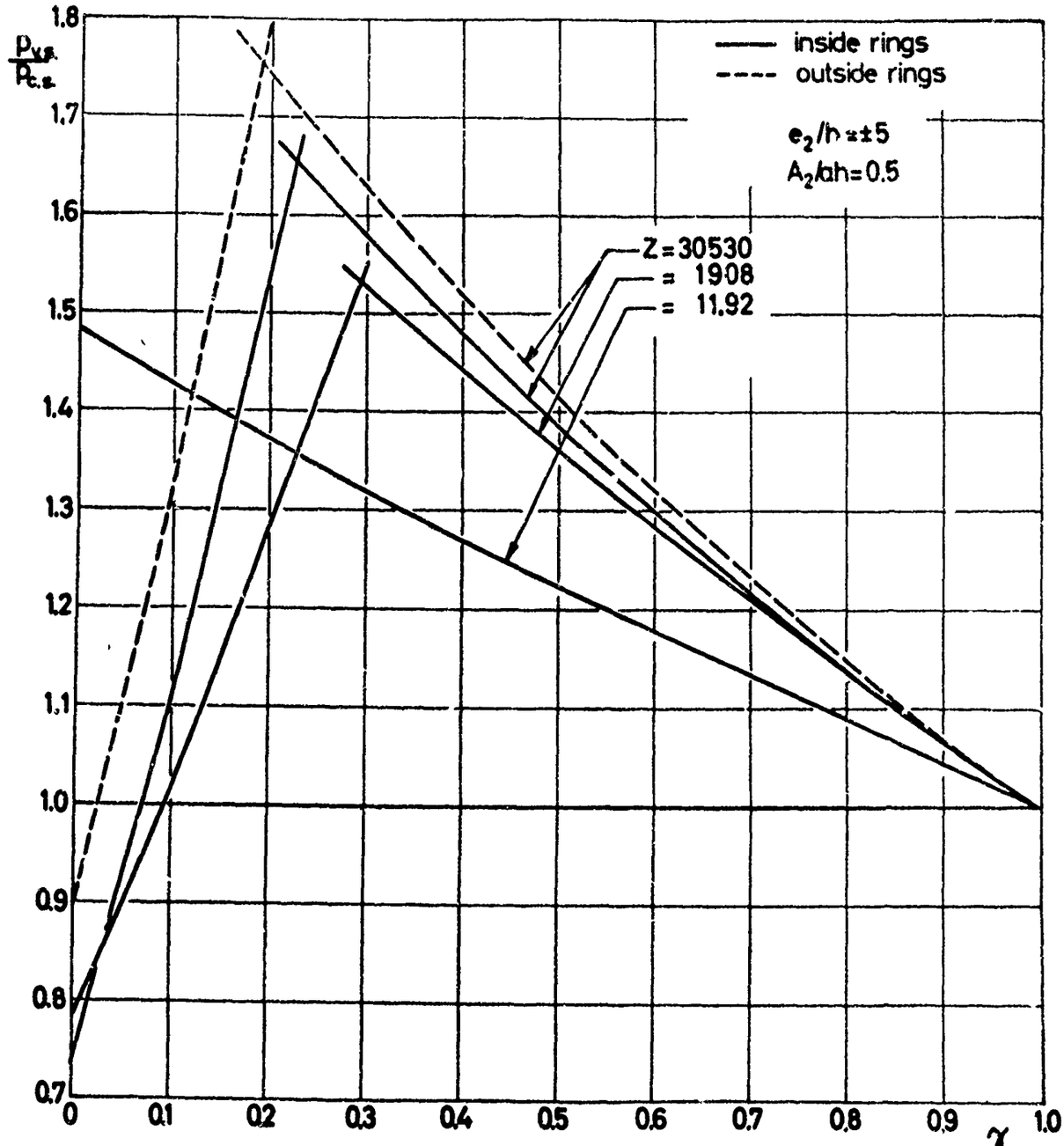

FIG. 10 THE INFLUENCE OF γ ON THE STRUCTURAL EFFICIENCY OF SHELLS WITH RINGS OF NON-UNIFORM HEIGHT (LATERAL PRESSURE)

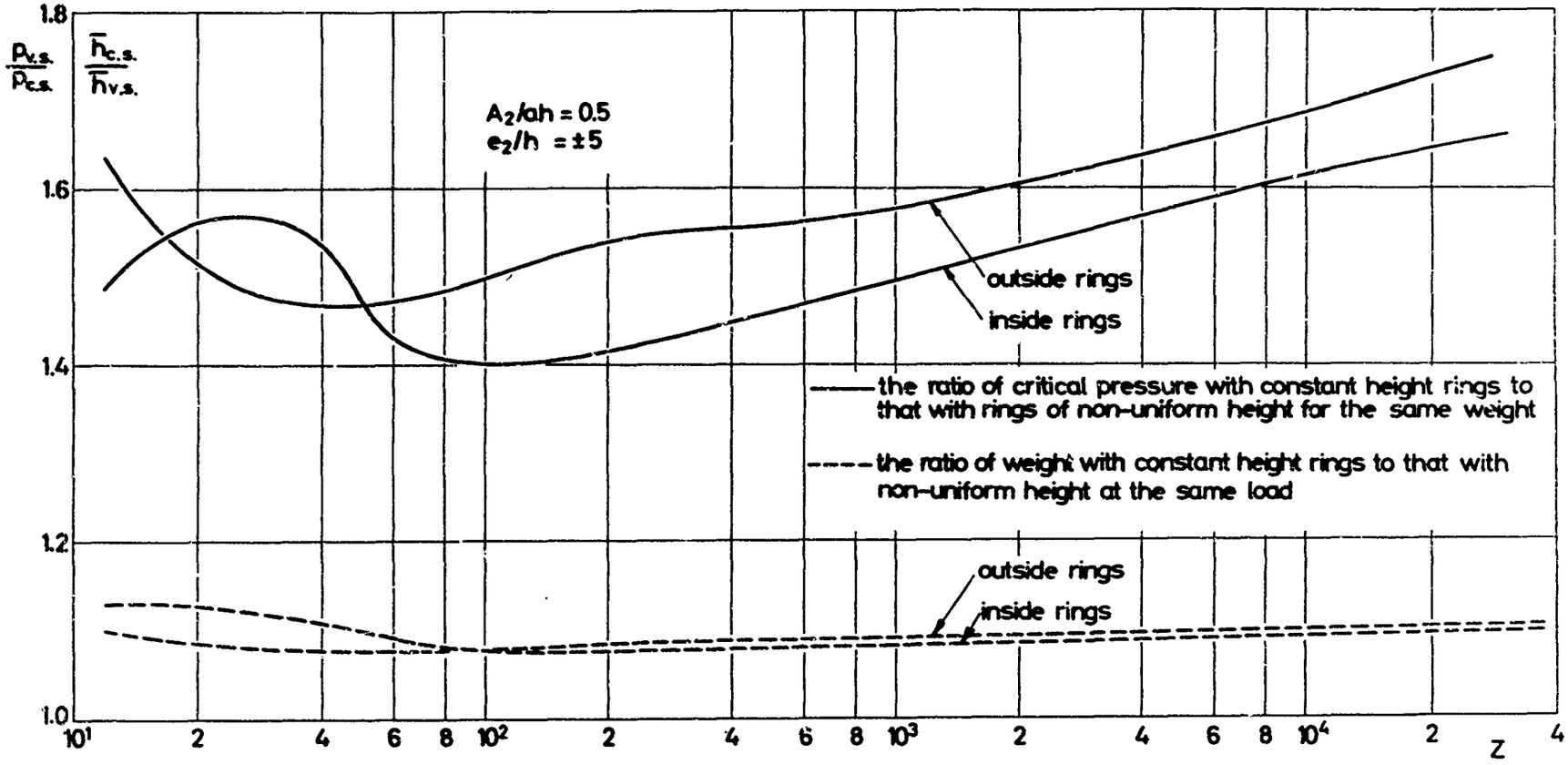

FIG. 11 GAIN IN LATERAL PRESSURE AND WEIGHT SAVING FOR SINUSOIDAL HEIGHT VARIATION AND OPTIMUM γ

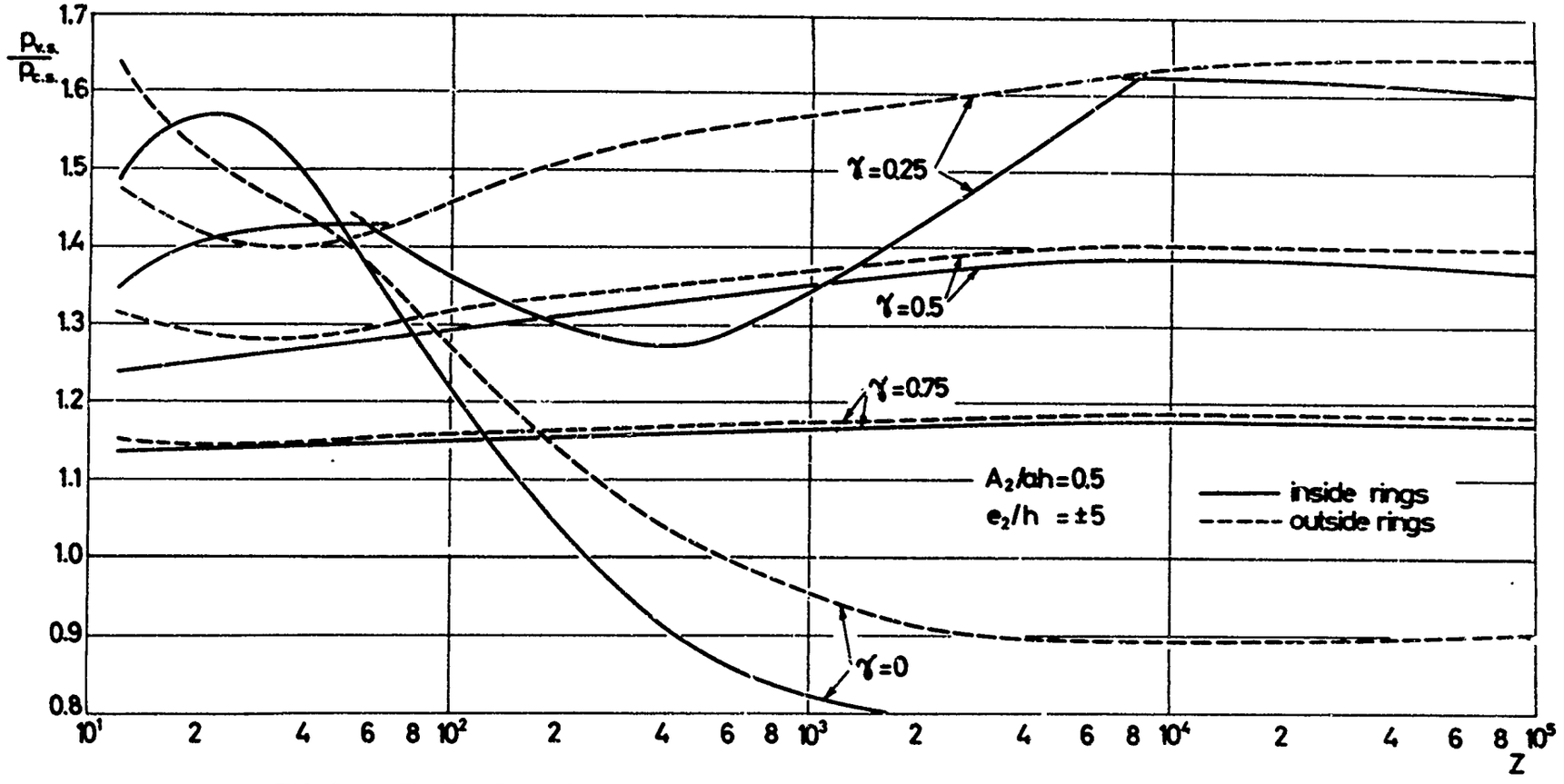

FIG.12 INFLUENCE OF SINUSOIDAL HEIGHT VARIATION OF RINGS ON LATERAL PRESSURE

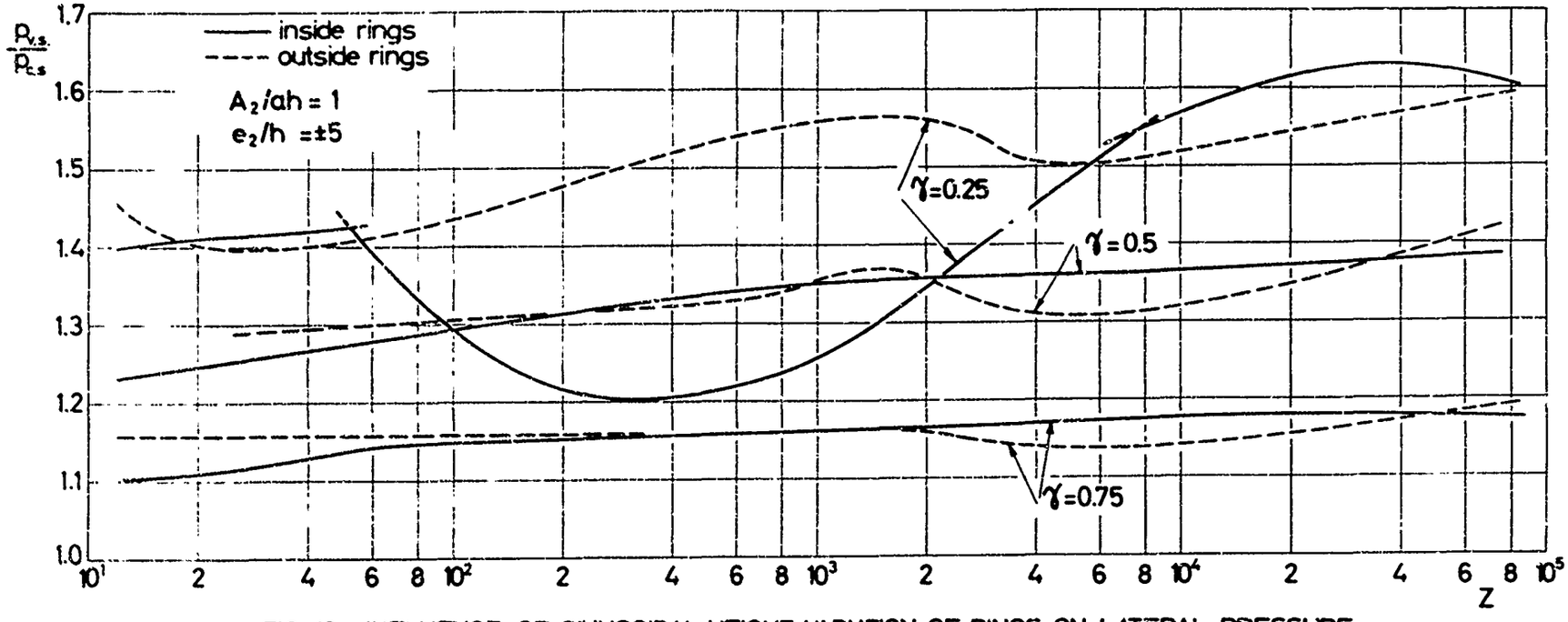

FIG. 13 INFLUENCE OF SINUSOIDAL HEIGHT VARIATION OF RINGS ON LATERAL PRESSURE

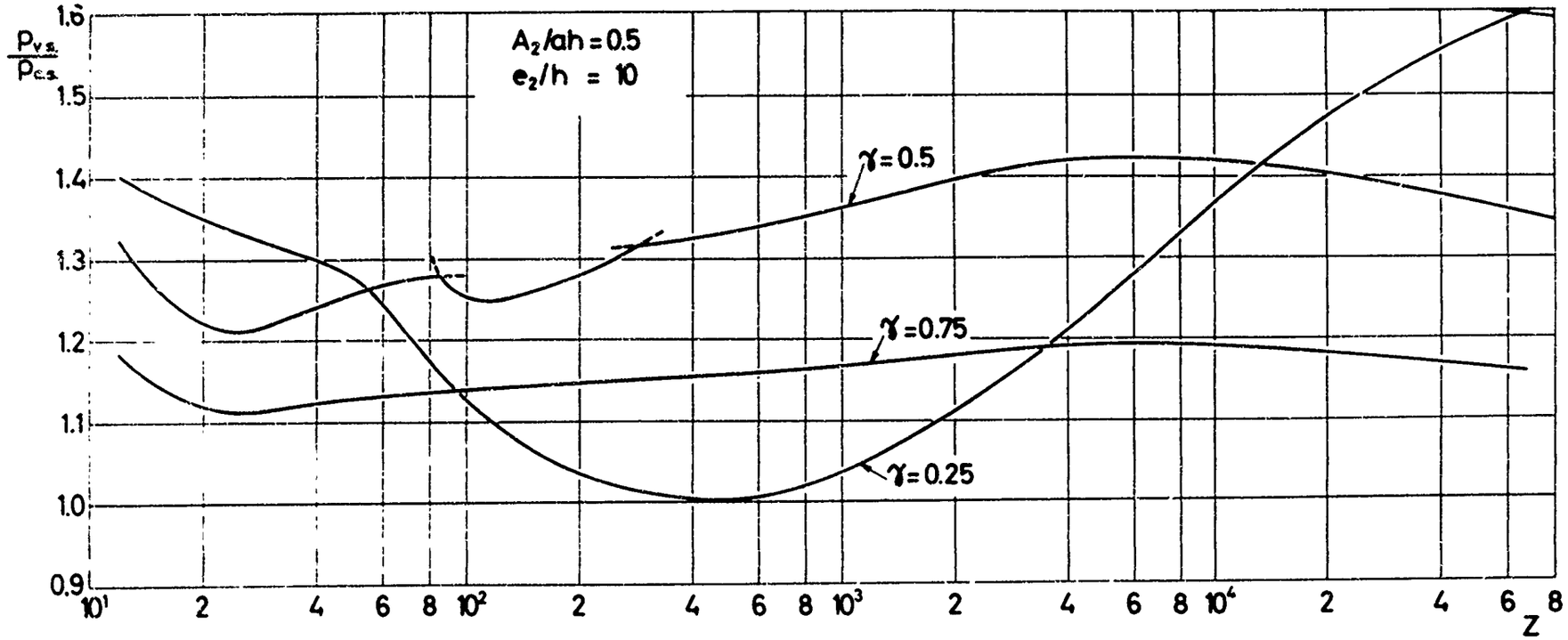

FIG. 14 INFLUENCE OF SINUSOIDAL HEIGHT VARIATION OF RINGS ON LATERAL PRESSURE

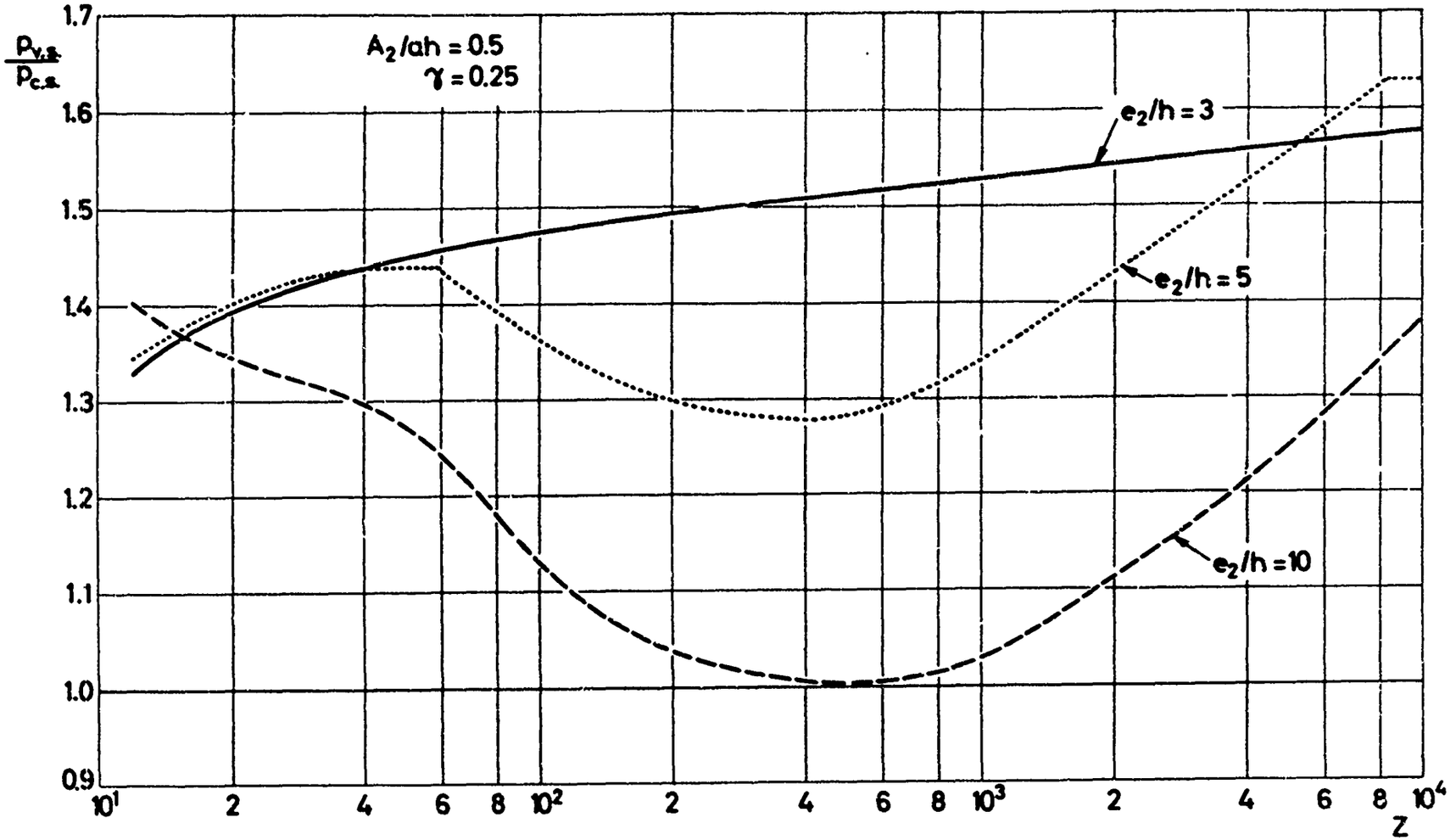

FIG. 15 EFFECT OF ECCENTRICITY ON THE STRUCTURAL EFFICIENCY OF RINGS WITH SINUSOIDAL HEIGHT VARIATION
(LATERAL PRESSURE)

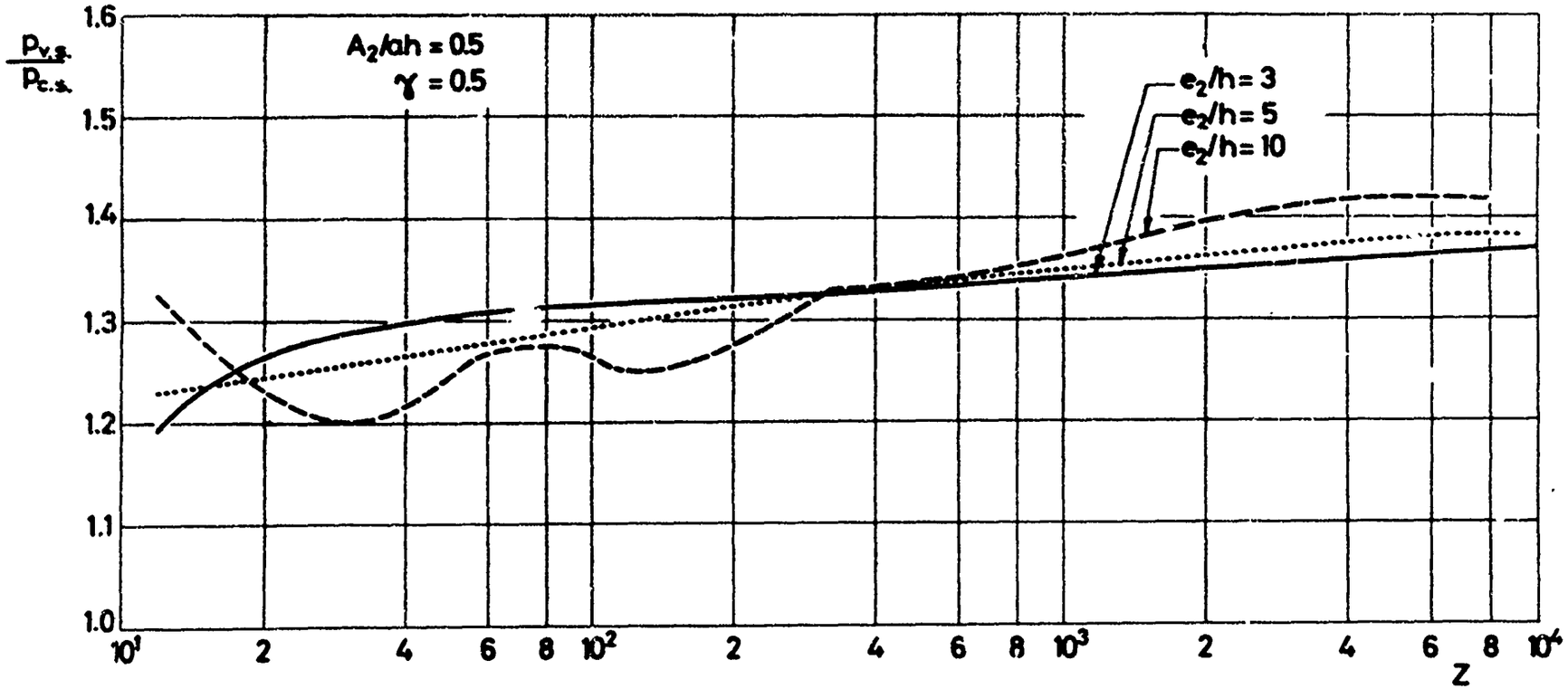

FIG. 16 EFFECT OF ECCENTRICITY ON THE STRUCTURAL EFFICIENCY OF RINGS WITH SINUSOIDAL HEIGHT VARIATION
(LATERAL PRESSURE)

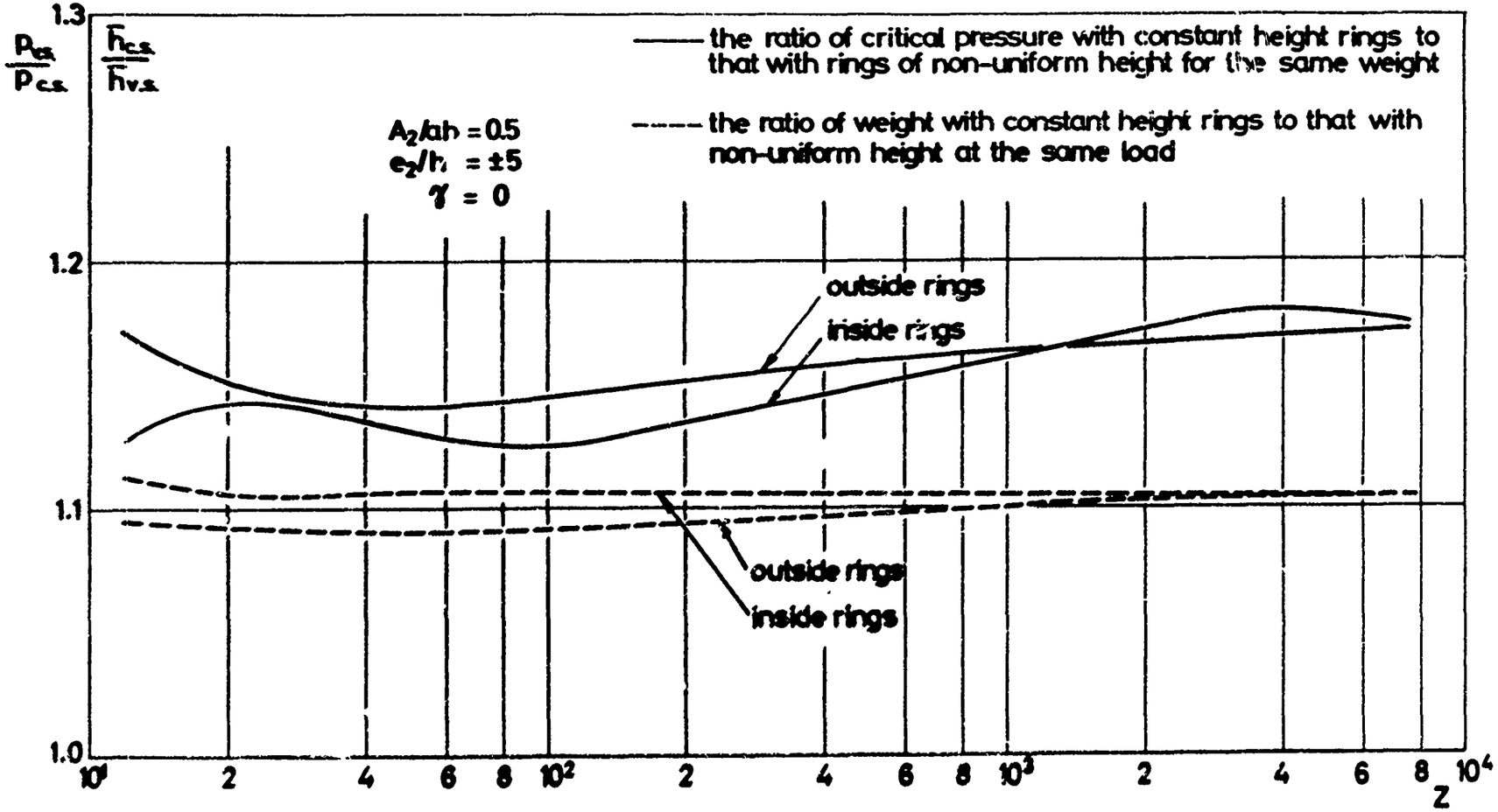

FIG. 17 GAIN IN LATERAL PRESSURE AND WEIGHT SAVING FOR SINUSOIDAL WIDTH VARIATION

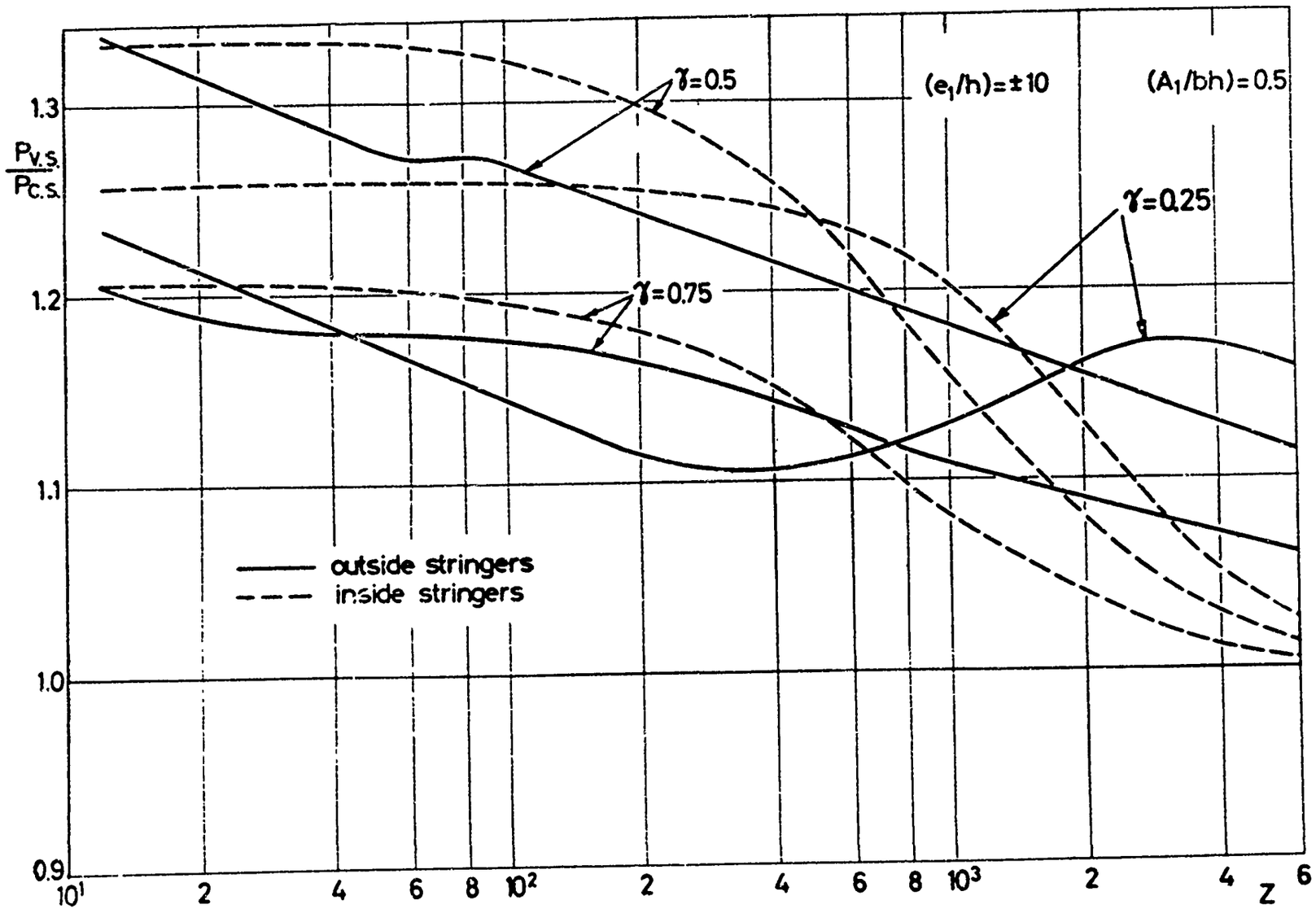

FIG.18 INFLUENCE OF SINUSOIDAL HEIGHT VARIATION OF STRINGERS ON BUCKLING LOAD (AXIAL COMPRESSION)

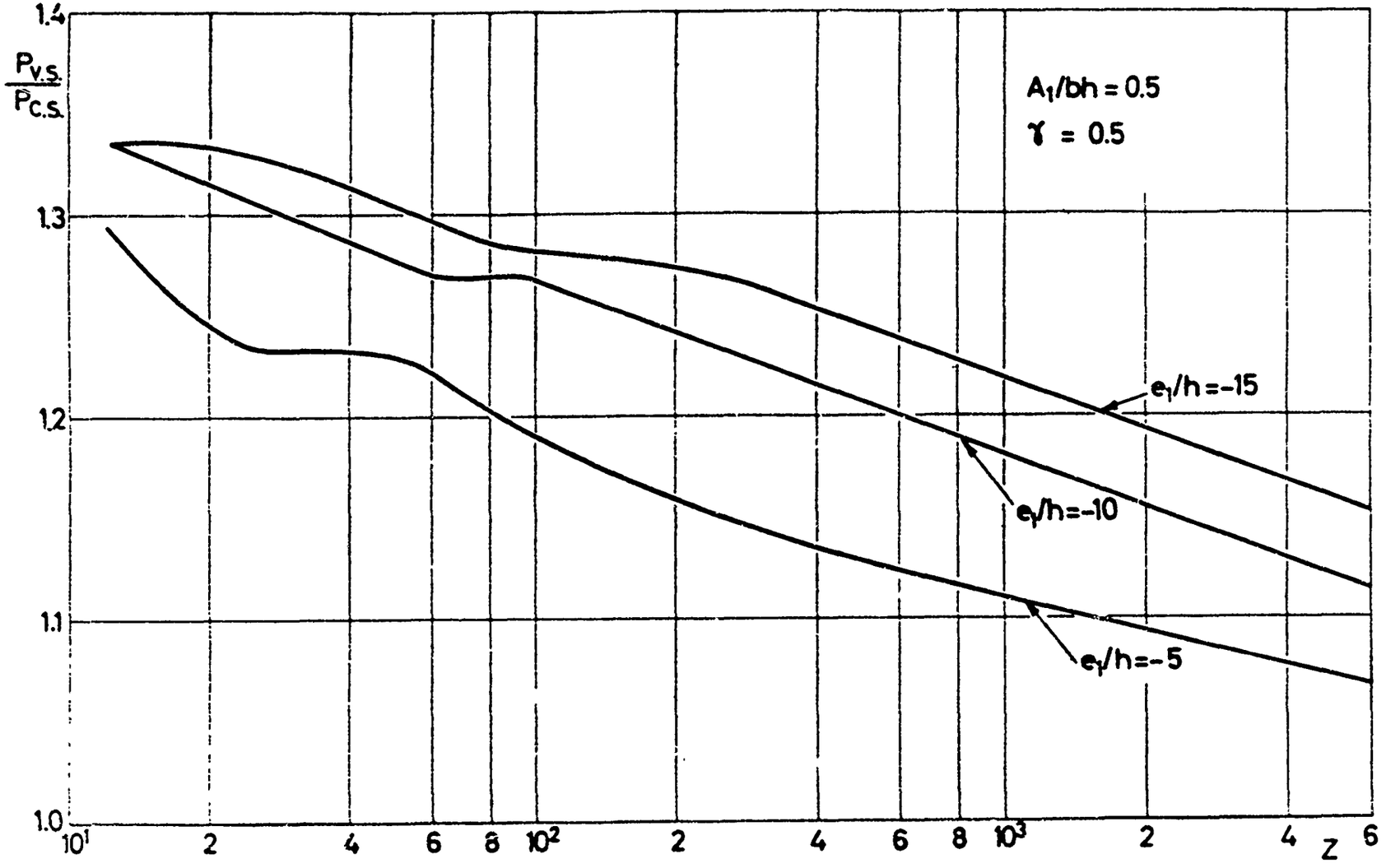

FIG. 19 EFFECT OF ECCENTRICITY ON THE RELATIVE STRUCTURAL EFFICIENCY OF STRINGERS WITH SINUSOIDAL HEIGHT VARIATION
(AXIAL COMPRESSION)

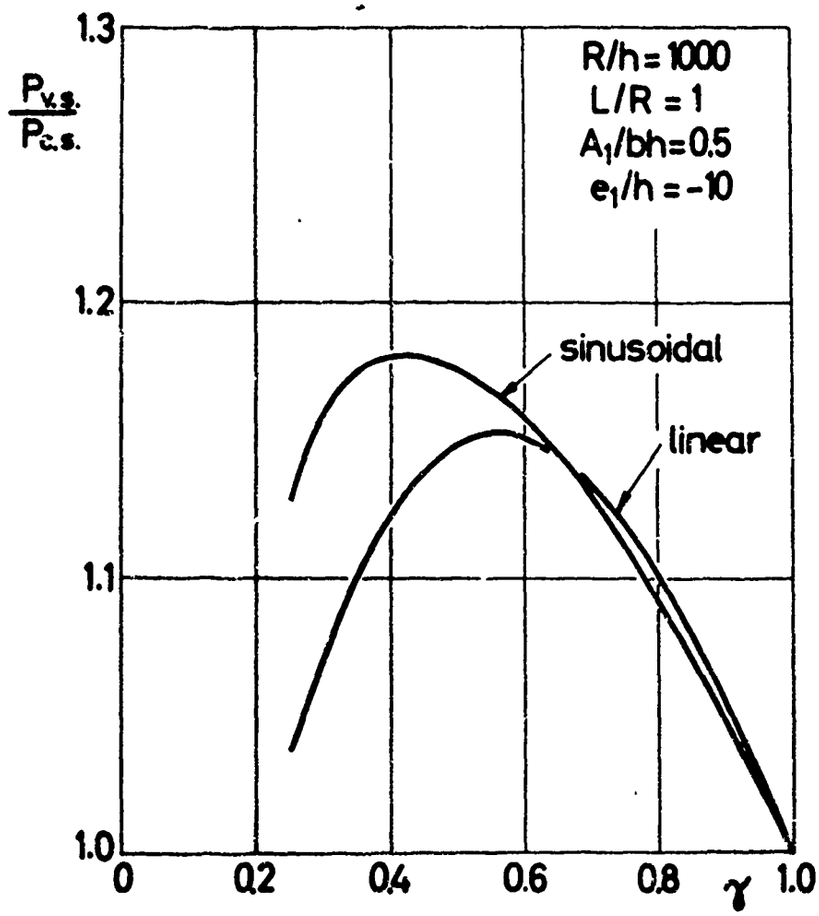

FIG. 20 THE INFLUENCE OF γ ON THE STRUCTURAL EFFICIENCY OF TWO TYPES OF STRINGER HEIGHT VARIATION (AXIAL COMPRESSION)

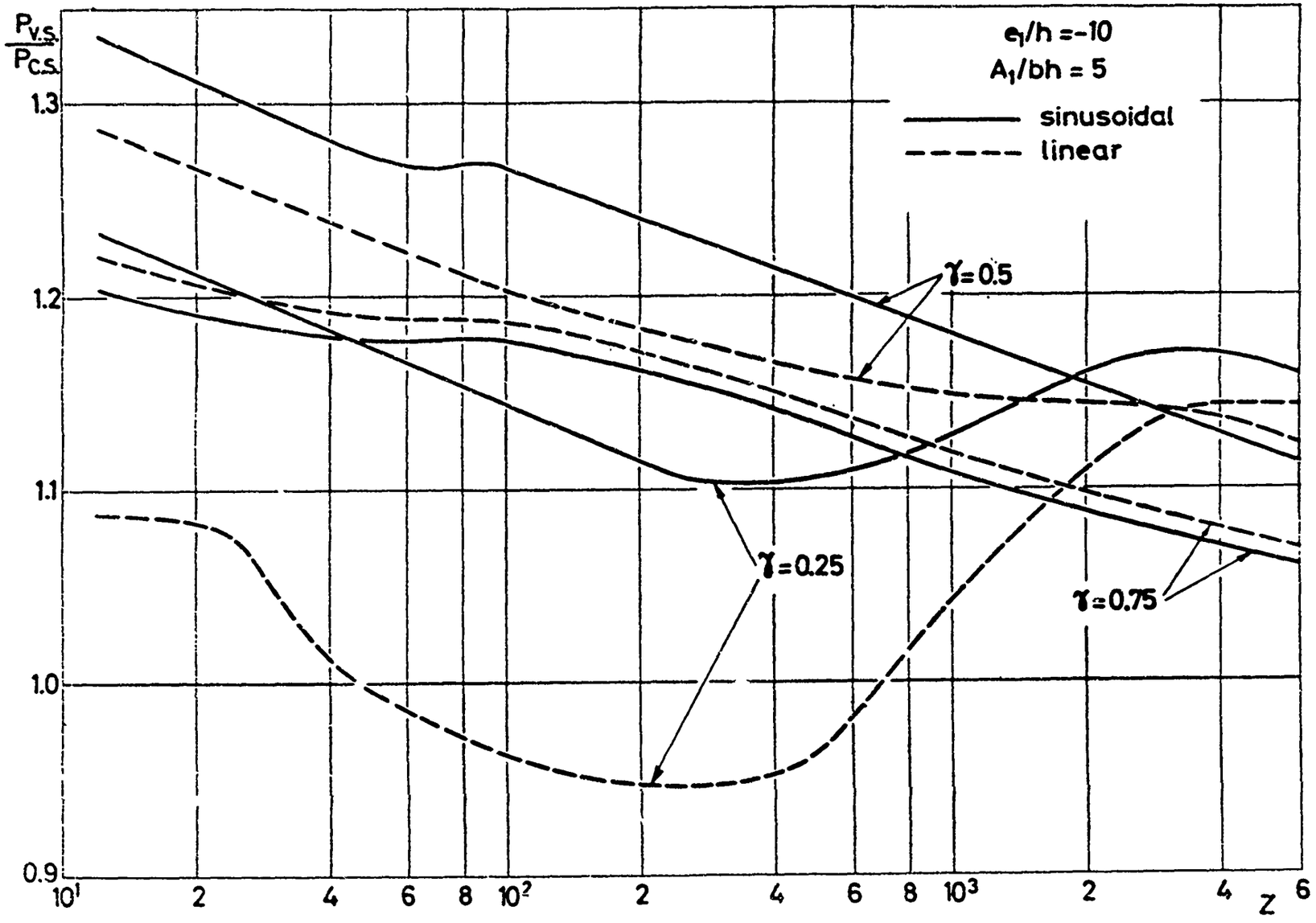

FIG. 21 COMPARISON OF STRUCTURAL EFFICIENCY OF LINEAR AND SINUSOIDAL HEIGHT VARIATION OF STRINGERS (AXIAL COMPRESSION)

(AXIAL COMPRESSION)

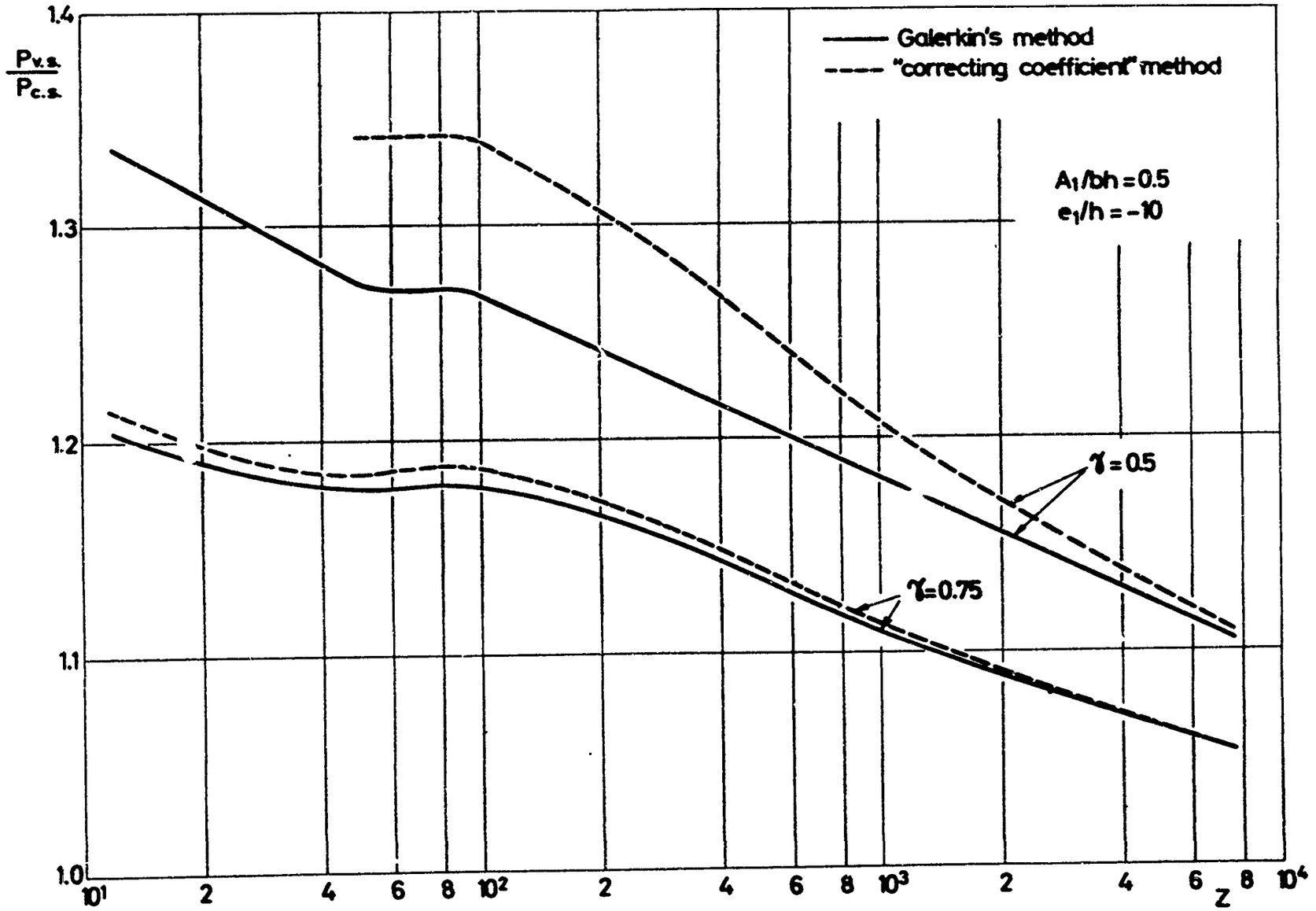

FIG. 22 COMPARISON OF SOLUTIONS BY THE GALERKIN METHOD AND THE METHOD OF CORRECTING COEFFICIENTS FOR SINUSOIDAL HEIGHT VARIATION OF STRINGERS (AXIAL COMPRESSION)

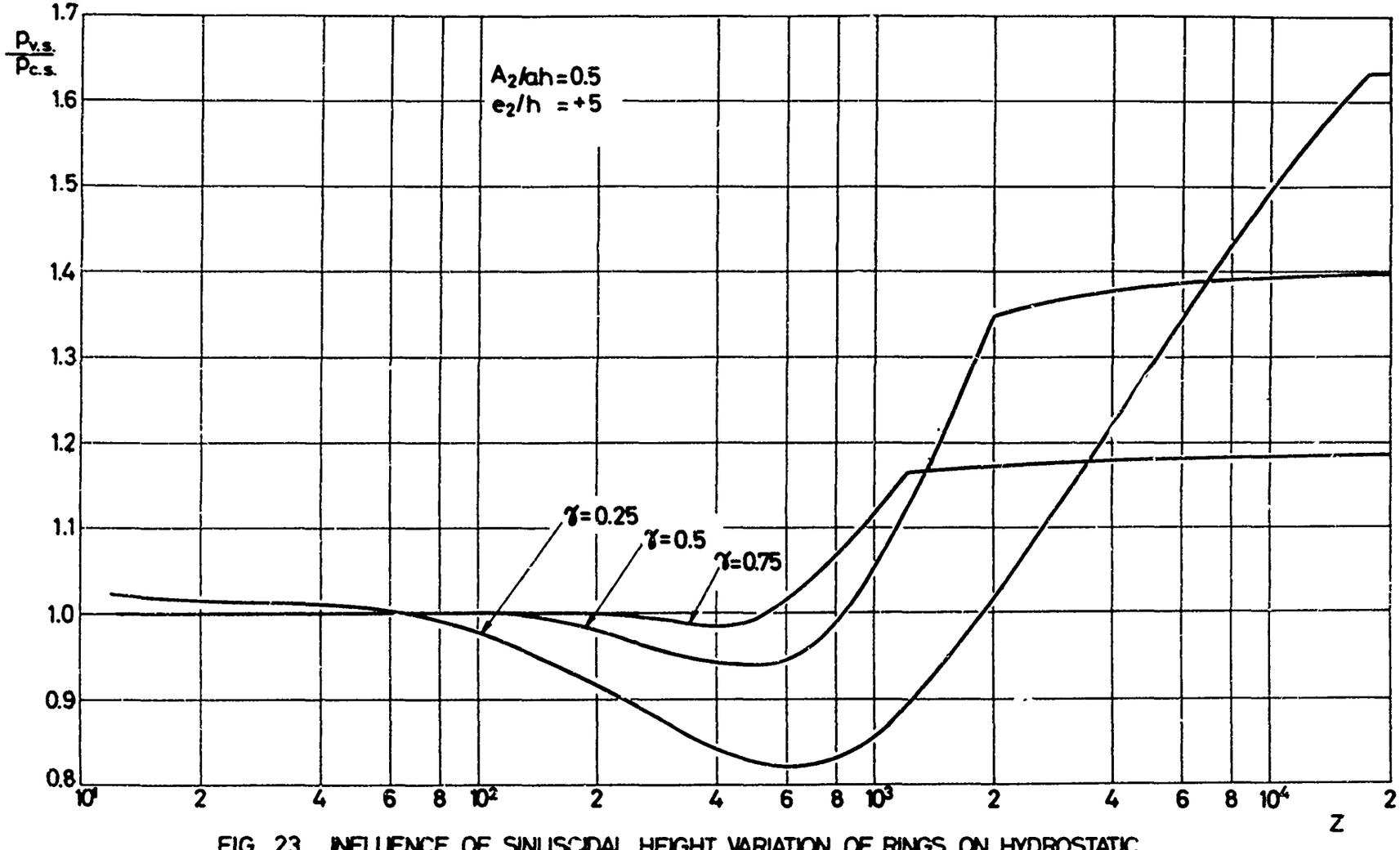

FIG. 23 INFLUENCE OF SINUSCIDAL HEIGHT VARIATION OF RINGS ON HYDROSTATIC PRESSURE

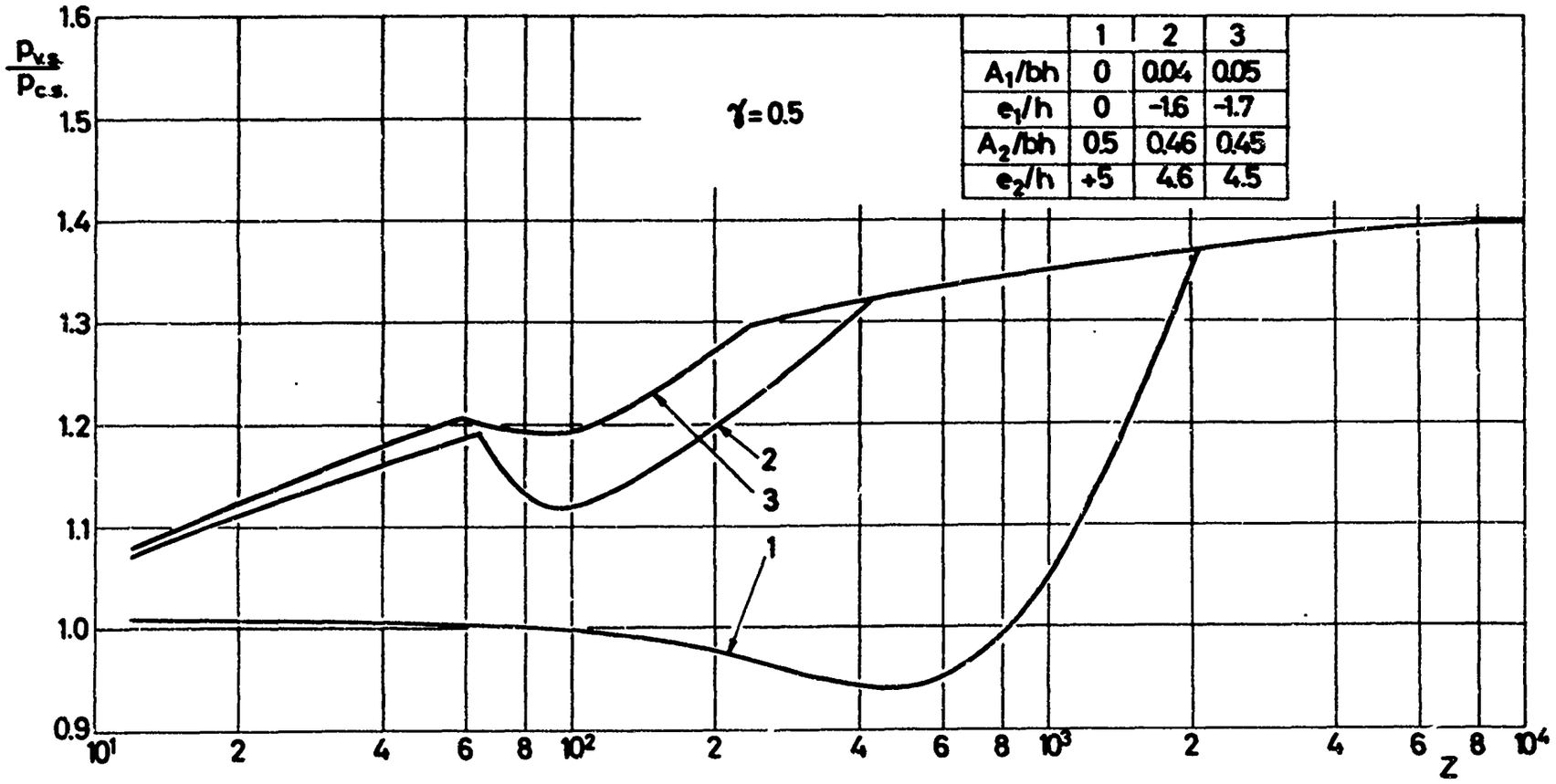

FIG. 24 INFLUENCE OF SINUSOIDAL HEIGHT VARIATION OF INSIDE RINGS WITH UNIFORM OUTSIDE STRINGERS ON HYDROSTATIC PRESSURE

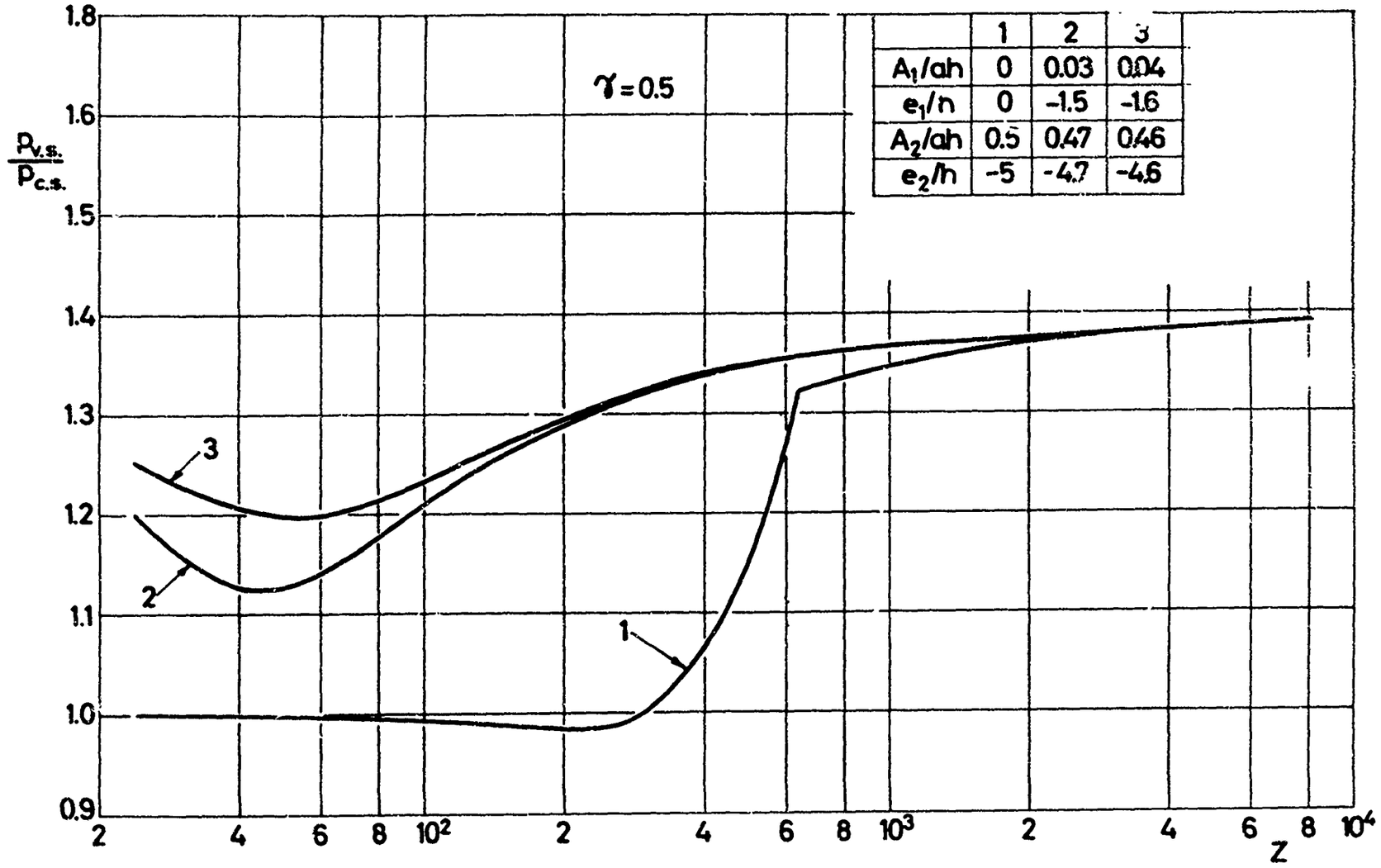

	1	2	3
A_1/ah	0	0.03	0.04
e_1/h	0	-1.5	-1.6
A_2/ah	0.5	0.47	0.46
e_2/h	-5	-4.7	-4.6

$\frac{P_{v.s.}}{P_{c.s.}}$

FIG. 25 INFLUENCE OF SINUSOIDAL HEIGHT VARIATION OF OUTSIDE RINGS WITH UNIFORM OUTSIDE STRINGERS ON HYDROSTATIC PRESSURE

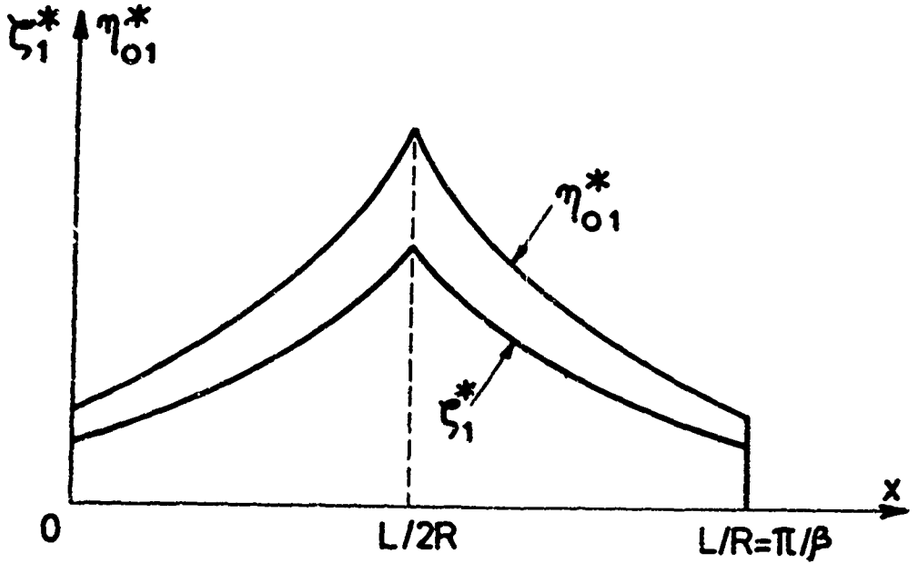

FIG. 26 TYPICAL VARIATION WITH A DISCONTINUITY IN SLOPE